

# Inertial **MEMS**

Principles and Practice

Volker Kempe

CAMBRIDGE

CAMBRIDGE

[www.cambridge.org/9780521766586](http://www.cambridge.org/9780521766586)

This page intentionally left blank

# **Inertial MEMS**

## **Principles and Practice**

A practical and systematic overview of the design, fabrication, and testing of MEMS-based inertial sensors, this comprehensive and rigorous guide shows you how to analyze and transform application requirements into practical designs, and helps you to avoid potential pitfalls and to cut design time.

With this book you'll soon be up to speed on the relevant basics, including MEMS technologies, packaging, kinematics and mechanics, and transducers. You'll also get a thorough evaluation of different approaches and architectures for design and an overview of key aspects of testing and calibration.

Unique insights into the practical difficulties of making sensors for real-world applications make this up-to-date description of the state of the art in inertial MEMS an ideal resource for professional engineers in industry, managers, and application engineers, as well as for students looking for a complete introduction to the area.

VOLKER KEMPE has more than 40 years of experience in research and development in both academia and industry. He led the microelectronics engineering department at Austria Mikro Systems for over 10 years. In 2003 he co-founded, and became Vice President of, SensorDynamics AG, and his current interests focus on the functionality, technology, and application of inertial MEMS.



# Inertial MEMS

## Principles and Practice

Volker Kempe  
*Sensor Dynamics AG, Austria*



**CAMBRIDGE**  
UNIVERSITY PRESS

CAMBRIDGE UNIVERSITY PRESS

Cambridge, New York, Melbourne, Madrid, Cape Town,  
Singapore, São Paulo, Delhi, Tokyo, Mexico City

Cambridge University Press  
The Edinburgh Building, Cambridge CB2 2RU, UK

Published in the United States of America by Cambridge University Press, New York

[www.cambridge.org](http://www.cambridge.org)

Information on this title: [www.cambridge.org/9780521766586](http://www.cambridge.org/9780521766586)

© Cambridge university Press 2011

This publication is in copyright. Subject to statutory exception  
and to the provisions of relevant collective licensing agreements,  
no reproduction of any part may take place without the written  
permission of Cambridge University Press.

First published 2011

Printed in the United Kingdom at the University Press, Cambridge

*A catalogue record for this publication is available from the British Library*

*Library of Congress Cataloguing in Publication data*

Kempe, Volker.

Inertial MEMS : principles and practice / Volker Kempe.

p. cm.

Includes bibliographical references and index.

ISBN 978-0-521-76658-6 (hardback)

1. Microelectromechanical systems. 2. Inertial navigation systems. 3. BioMEMS. I. Title.

TK7875.K46 2011

629.04'5 – dc22 2010037668

ISBN 978-0-521-76658-6 Hardback

---

Cambridge University Press has no responsibility for the persistence or  
accuracy of URLs for external or third-party internet websites referred to  
in this publication, and does not guarantee that any content on such  
websites is, or will remain, accurate or appropriate.

---

# Contents

	<i>Preface</i>	<i>page</i> xiii
	<i>Acknowledgments</i>	xv
	<i>Notation</i>	xvi
1	Introduction	1
	1.1 A short foray through the pre-MEMS history	1
	1.2 Applications and market	6
	1.3 The ingredients of inertial MEMS	9
	References	11
2	Transducers	13
	2.1 Anisotropic material properties, tensors, and rotations	13
	2.1.1 Stress, strain, and piezoresistivity	14
	Hooke's law	14
	Normal stresses	14
	Shear stresses	15
	Stress and strain tensors	17
	The stress–strain relation for anisotropic materials	21
	The piezoresistance of silicon	24
	2.1.2 Rotation of coordinate systems	25
	Coordinate frames	26
	The rotation tensor	27
	Transformation of tensors of second order	30
	2.2 Piezoresistive transducers	33
	2.2.1 Piezoresistors	33
	2.2.2 Piezoresistors on silicon	34
	Thin piezoresistors	35
	Temperature compensation in piezoresistors	36
	2.2.3 Piezoresistors on polysilicon	38
	2.3 Piezoelectric transducers	39
	2.3.1 The piezoelectric effect	39
	2.3.2 Piezoelectric equations	42
	Piezoelectric sensors in MEMS	43

---

2.4	Capacitive transducers	47
2.4.1	Electrostatic forces	49
2.4.2	Parallel-plate capacitors	51
	Capacitance sensing	51
	The pull-in effect	53
2.4.3	Tilting-plate capacitors	55
	Nonlinear distortions	56
	Instabilities of a singular tilting plate	58
	Instabilities of the tilting capacitance pair	58
2.4.4	Comb capacitors	62
	Unidirectional linear combs	62
	Bidirectional actuation	65
	Radial combs	66
	Frame-based capacitors	67
2.4.5	Levitation	69
	Comb levitation	69
	Levitation in drive combs	71
	Reduction of levitation forces	73
	References	75
3	Non-inertial forces	79
3.1	Springs	79
3.1.1	Beams	80
3.1.2	The stiffness matrix	81
3.1.3	The bending equation for beams	82
	Internal forces and moments	83
	Differential relations of a bent beams	83
3.1.4	Cantilever beams	87
	Cantilevers under different loads	87
	Skew beam bending and asymmetric suspensions	90
	Residual stress in bending beams	93
3.1.5	Torsion springs	96
	Cylindrical torsion bars	96
	Torsion bars with arbitrary cross-section	97
	Rectangular bars	100
	Cylindrical bars	101
3.1.6	Stress concentration	101
3.1.7	Suspensions	103
	Parallel and serial spring connections	103
	Beam chains	104
	Plate suspension	105
3.2	Damping forces	108
3.2.1	Fluid-flow models	108

---

	Continuous viscous flow	111
	Viscosity of gases	112
	Continuous-flow equations	114
3.2.2	Slide damping	117
	Couette flow for slowly moving plates	118
	Stokes flow for rapidly oscillating plates	120
3.2.3	Squeeze damping	124
	Reynolds' equation	125
	Low-frequency squeeze damping	127
	High-frequency squeeze damping	131
	The impact of perforation	137
3.2.4	Drag forces	143
3.2.5	Free molecular flow	145
3.2.6	Structural damping	147
	References	148
4	MEMS technologies	152
4.1	Microfabrication of inertial MEMS	153
4.1.1	Basic microelectronic fabrication steps	154
	Deposition	155
	Patterning	159
	Doping	161
4.1.2	Etching	162
	Isotropic wet etching	162
	Anisotropic wet etching	164
	Electrochemical etch stop	167
4.1.3	Dry etching	168
	Reactive-ion etching	168
	Deep reactive-ion etching	170
4.2	Wafer bonding	172
4.2.1	Zero-level packaging and wafer bonding	172
4.2.2	Wafer-bonding processes	174
	Fusion bonding	175
	Anodic bonding	176
	Glass-frit bonding	177
	Metallic-alloy seal bonding	179
	Polymer bonding	180
	Thermocompression bonding	180
4.3	Integrated processes	180
4.3.1	Bulk micromachining	182
4.3.2	Surface micromachining	184
	A thick polysilicon process	185
	Cavity sealing using SMM	188

	4.3.3	SOI-MEMS processes	189
		MEMS prototyping processes	192
	4.3.4	CMOS-MEMS	192
		Pre-CMOS MEMS	193
		Intra-CMOS MEMS	195
		Post-CMOS MEMS	196
		References	199
5		First-level packaging	205
	5.1	FLP packages	206
	5.2	FLP technologies	209
		5.2.1 Dicing and die separation	210
		5.2.2 Die attachment	211
		Packaging materials	212
		Die-attachment-induced stress	213
		5.2.3 Electrical interconnection	217
		5.2.4 Encapsulation	220
		Overmolded plastic packages	221
		Pre-molded plastic packages	223
		References	225
6		Electrical interfaces	227
	6.1	Sensing electronics – building blocks	228
		6.1.1 The MOS transistor	229
		Drain current	229
		The small-signal model	231
		6.1.2 Operational and transconductance amplifiers	234
		A simple transconductance amplifier	234
		Models of operational and transconductance amplifiers	236
		The real Op Amp	240
		Instrumentation amplifiers	246
	6.2	Sensor interfaces	247
		6.2.1 Resistive interfaces	247
		6.2.2 Piezoelectric interfaces	249
		6.2.3 Capacitive interfaces	253
		Principles of capacitive sensing	254
		Current sensing	255
		Voltage sensing	258
		Charge sensing	259
		Comparison and improvements	260
		Switched-capacitor sensing	260
	6.3	Data converters	266
		6.3.1 Sampling and hold	266

6.3.2	Single-sample conversion in the amplitude domain	268
6.3.3	Time-domain conversion	269
	Pulse-width and pulse-density modulation	269
	$\Sigma\Delta$ Converters	271
	References	280
7	Accelerometers	283
7.1	General measurement objectives	283
7.2	The spring–mass system	284
7.2.1	The transfer functions	286
	The trade-off between sensitivity and bandwidth	291
7.2.2	Accelerometer imperfections	292
	A simplified accelerometer model with imperfections	296
	Cross-coupling	297
7.2.3	Accelerometer feedback control	298
	The linearized feedback model	300
	The signal-to-noise ratio	305
	Closed-loop dynamics	307
7.2.4	Feedback control with nonlinear actuators	309
	Bidirectional capacitive actuators	310
	Single-sided actuators	312
	Linearization and embedded $\Sigma\Delta$ converters	313
7.3	Resonant accelerometers	319
7.3.1	Resonant beams	320
	Resonance vibration – exact solution	320
	Resonance frequencies by the energy method	323
7.3.2	Resonant accelerometer systems	324
7.4	Beam accelerometers	326
7.4.1	Beam dynamics	328
	The principle of virtual work	329
	Eigenmode expansion	330
	Damping and electrostatic forces	332
	Static deflection	333
7.4.2	Model implementation	333
	The impact of nonlinear damping	335
	Feedback control	336
7.5	Various other accelerometer principles	337
7.5.1	Tunneling accelerometers	337
7.5.2	Convective and bubble accelerometers	339
7.6	From 1D to 6D accelerometers	341
7.6.1	1D accelerometers	342
	Piezoresistive accelerometers	343
	Capacitive accelerometers	346

	Piezoelectric accelerometers	348
7.6.2	2D and 3D accelerometers	350
	Parallel implementation	350
	2D and 3D accelerometers with multi-DOF sensing elements	353
7.6.3	6D accelerometers	355
	References	358
8	Gyroscopes	364
8.1	Some basic principles	364
8.2	Kinematics of gyroscopes	367
8.2.1	Platform rotation and angular velocity	369
8.2.2	Body rotation in a non-inertial system	371
8.2.3	The angular-momentum theorem	373
8.2.4	The momentum equation	375
8.2.5	The small-angle approximation	376
8.3	The performance of gyroscopes	378
8.4	Rate-integrating gyroscopes	380
8.4.1	Two-DOF gyroscopes	380
8.4.2	The principle of angular gyroscopes	381
8.4.3	An imperfection model	385
8.4.4	Imperfection in angular gyroscopes	387
8.4.5	Gyroscope control	388
8.5	Rate gyroscopes	389
8.5.1	System architecture	391
	The drive resonator	393
	Sensing	393
8.5.2	Resonance sensing	395
8.5.3	Non-resonant sensing	398
8.5.4	Noise	400
8.5.5	The zero-rate output	402
	Mechanical bias sources	403
	Q-bias	405
	The impact of transducer imperfections	408
	R-bias	409
	Other bias sources	410
8.5.6	Bias stability	411
8.5.7	Acceleration suppression and tuning forks	413
	Anti-phase-driven identical gyroscopes	414
	Tuning-fork gyroscopes	415
8.5.8	Drive-motion control and spring nonlinearities	418
	The phase-locked loop	418
	The amplitude loop	419
	Spring nonlinearities and the resonator transfer function	421

8.6	Gyroscope architectures	424
	8.6.1 Mode-decoupling architectures	424
	8.6.2 <i>z</i> -Gyroscopes	424
	Mode decoupling by frame-based architectures	424
	Doubly decoupled <i>z</i> -gyroscopes	427
	8.6.3 In-plane-sensitive gyroscopes	429
	In-plane-sensitive linear gyroscopes	429
	Linear-rotatory gyroscopes	430
	8.6.4 Torsional gyroscopes	431
	1D torsional gyroscopes	432
	Decoupled torsional gyroscopes	433
8.7	Non-planar MEMS gyroscopes	438
	8.7.1 Beam gyroscopes	438
	8.7.2 Quartz tuning forks	440
	8.7.3 Ring gyroscopes	441
	8.7.4 Bulk acoustic-wave gyroscopes	443
8.8	2D and 3D gyroscopes and ways towards a 6D IMU	444
	8.8.1 Single-mass multiple-DOF inertial sensors	445
	Gyroscope-free, single-mass IMUs	445
	Single-mass, gyroscope-based IMUs	445
	5D inertial sensors	447
	8.8.2 2D gyroscopes	448
	8.8.3 3D gyroscopes	449
	A fully decoupled 3D gyroscope and extension towards an IMU	450
	References	452
9	Test and calibration	460
	References	464
	<i>Concluding remarks</i>	466
	References	467
	<i>Index</i>	468

*The color plates are to be found between pages 240 and 241.*



# Preface

Inertial microelectromechanical sensors – commonly abbreviated to inertial MEMS – have a history of more than two decades of intense research, development, and commercialization. Sometimes unperceived, they left the shadow of military and space-related utilities and entered daily life hidden in products surrounding us. Cars with airbag-release sensors and electronic stability control have become a matter of course. Activity monitoring of pacemaker patients and stabilization of platforms such as transport robots and cameras are now improving our quality of life. The creation of easy-to-use human–machine interfaces has helped many people to conquer complicated equipment around us, not only computer games. The penetration of inertial MEMS – often merged with other sensor systems – into new application areas is a trend that is still gaining momentum.

The intention of this book is to reflect the interdisciplinary complexity of inertial MEMS. It will try to give a systematic survey of the design, fabrication, and performance evaluation of MEMS-based inertial sensors, with emphasis on the practical problems arising from the impact of technological imperfections and of often harsh environmental conditions. A product going to the market has to be guaranteed to have a certain level of reliability against failure throughout its lifetime.

The basic concepts and the theoretical background of inertial measurements will be presented. However, the book has evolved not from academic activity but rather from conceptual and development work within industry. It is intended to address the symbiosis of practice and theory. Consequently, the analysis and transformation of application requirements into design concepts plays a significant role. Considerable space is devoted to the analysis and modeling of parasitic effects, of shock and vibration robustness, of the stability of the main performance parameters and so on, since this is necessary for practical work.

The book contains nine chapters. Six of them – including the introduction – cover various aspects of MEMS, with a special focus on inertial MEMS. The first chapter describes the most important transducers and their properties. The second one is dedicated to non-inertial forces such as spring forces and damping forces that play a crucial role for designing inertial MEMS. The next two chapters cover the main MEMS technologies, including packaging, while the electronic interfaces are presented in a further chapter. These six chapters may be

interesting not only for people working with inertial MEMS but also for everybody who is looking for a general introduction into mechanical MEMS.

The following two main chapters are devoted to the two representatives of inertial MEMS – accelerometers and gyroscopes. Here the focus is on the basic principles, the methods and models to describe the dynamic behavior, and a comprehensive presentation of different approaches and architectures, including their pros and cons. A short overview on test and calibration is added as a separate chapter.

The book is written on an engineering level. Where possible, effects and processes are described analytically by mathematical models in order to impart a feeling for the order of magnitude of different effects.

The book should be useful not only for specialists developing, manufacturing, and using inertial sensors but also for people working in the application field, for product managers, and for sales people looking for background knowledge in their area. The book can serve as a starting point for further academic investigations, for instance in the area of shock-impact analysis of an entire packaged gyro, including the effect of signal processing.

In the experience of the author, many engineers, physicists, and mathematicians are thankful for an exact but comprehensible presentation of the complex and difficult world of MEMS-based inertial sensors, where the effects and models behind the practical problems are reflected without improper simplifications or phenomenological descriptions. The book is a modest attempt to meet some of these challenges. Having worked with many specialists in the production, testing, and design of inertial sensors, the author is convinced that the book can meet actual needs, and hopes to elicit the broad interest of practitioners and scientists in this area. For interested people, including students, the book may also serve as an introduction to the world of mechanical MEMS.

# Acknowledgments

I would like to express my gratitude to all my colleagues at SensorDynamics AG (Austria) and the Institut für Silizium Technologie (ISIT) of the Fraunhofer Society (Germany) for creating an atmosphere that has helped to solve the manifold problems of MEMS industrialization. I would like to thank the ‘Inertial Micro Sensor Systems’ team, with whom I have had the great privilege of working even during the childhood of the newly founded company SensorDynamics AG. This time was most fruitful, flooding us all with new problems and insights into how to solve them.

My thanks go to my colleagues from SensorDynamics for providing me with such necessary illustrative material for the book as SEM photographs and measurement plots. Gottfried Fraiss, Manfred Heller, Christian Rossadini, Jörg Schönbacher, Ute Stotter, and Johann Wagner prepared a lot of material from which I could select the most appropriate items. Gerd Radl and his team accompanied me during all my mistakes with new hardware and software.

Drago Strle from the University of Ljubljana deserves my special thanks for the close cooperation throughout all  $\Sigma\Delta$ -related issues. Peter Merz from the ISIT gave me invaluable feedback on all technology-related questions. Professor Karl Wohllhart from the University of Graz helped me to gain a deeper understanding of the kinematics of gyroscopes. Hanno Hammer took on the burden of proof-reading the first chapters and supplying me with valuable feedback.

Last but not least, warmest thanks go to my family for supporting me despite all the personal loads that each of us has had to carry. Julia and Oded helped me to resolve quickly the countless difficulties in adapting appropriate document-creating tools to my needs. Vera, Ian, and Marius gave valuable advice on English phrasing. My dear wife took on additional duties despite her own excessive workload in working with very ill patients. Thank you.

# Notation

1. A convention employed in this book is the slightly lax usage of “ $s$ ” as differential operator,  $s = d/dt$ , as argument of the Laplace transformation, and as argument of the Fourier transformation,  $s = j\omega$ . The case-dependent unambiguous or multivalent meaning is usually clear from the context. Accordingly, a filter function is described by  $f = f(s)$ , which means that in a transfer function this expression has to be interpreted as a Laplace or Fourier transformation and within a differential equation as a rational fraction of two polynomial differential operators. Correspondingly, a variable like  $x$  has to be treated as a representant in the time domain if  $s = d/dt$  is supposed, or as a Laplace/Fourier-transformed function if  $s$  is meant as the argument of such a transformation.
2. Unless stated otherwise, coordinate systems pertain to the platform carrying the inertial sensor. In this case the  $x$ - and  $y$ -axes lie in the plane of the platform, while  $z$  is the out-of-plane axis. Out-of-plane and  $z$ -axis orientation are used synonymously.

# 1 Introduction

---

*An inertial sensor is an observer who is caught within a completely shielded case and who is trying to determine the position changes of the case with respect to an outer inertial reference system.*

Inertial sensors exploit inertial forces acting on an object to determine its dynamic behavior. The basic dynamic parameters are acceleration along some axis and the angular rate. External forces acting on a body cause an acceleration and/or a change of its orientation (angular position). The rate of change of the angular position is the angular velocity (angular rate). A speedometer is not an inertial sensor because it is able to measure a constant velocity of a body that is not exposed to inertial forces. An inertial sensor is unable to do so; however, if the initial conditions of the body are known, their evolution can be calculated by integrating the dynamic equation on the basis of the measured acceleration and rate signals.

In the overwhelming majority of practical applications, such as vibrational measurements, active suspension systems, crash-detection systems, alert systems, medical activity monitoring, safety systems in cars, and computer-game interfaces, the short-term dynamic changes of the object are of interest. But there are also many applications where inertial sensors are used for determination of the positions and orientations of a body, as in robotics, general machine control, and navigation. Owing to the necessity of integrating the corresponding dynamic equations, the accuracy requirements in these applications are usually higher because the measurement errors and instabilities of the sensors are accumulated over the integration time. Often inertial sensors are used in conjunction with other measurement systems, as in the case of robotics, where they are used together with position and force/torque sensors, or in the case of the integration of Inertial Navigation Systems (INS) with Global Positioning Systems (GPS) in cars. The accuracy of INS measurements can be improved significantly by correcting them with the GPS data using Kalman filtering procedures. The INS can then aid navigation even when the GPS is degraded or interrupted because of jamming or interference.

## 1.1 A short foray through the pre-MEMS history

The history of inertial sensors is relatively short. Despite the fundamental role played by inertial sensors in controlling the movement of a body, very little is

known about early applications. This is even more remarkable given that most of the ingredients for building acceleration and angular-rate sensors, such as fine mechanics and precise spring technologies, were available from the late Middle Ages on and were used in the construction of, for instance, beautiful precision clocks.

### *Accelerometers*

One of the most likely reasons for the late appearance of acceleration sensors (or “accelerometers” for short) was the lack of indicator technologies, or, in modern phrasing, the lack of interfaces. This is certainly the reason why some former applications of acceleration switches that needed only very simple mechanical interfaces can be found. An acceleration switch initiated an action at a certain level of acceleration, as in the activation of a detonator in some bombs during the First World War.

The first commercial accelerometer for broader application is credited to B. McCollum and O. S. Peters and was developed around 1920 [McCullom and Peters 1924]. It was based on a tension–compression resistance of a Wheatstone half-bridge where the resistances were formed by carbon rings. The next technological step was the use of strain-gauge transducers starting from around 1938, followed by the introduction of piezoelectric and piezoresistive transducers at the end of the 1940s. These transducers could capture the forces caused by the displacement of an elastically mounted mass within the sensor structure. Miniaturization and the high robustness of this type of sensor paved the way for broad applications in industry, terrestrial transport, aerospace, military uses, seismology, science, and so on. The piezoelectric and piezoresistive transducer principles were also among the first to be employed at the beginning of the entry into the world of inertial microelectromechanical systems (MEMS) – the world of the combination of micrometer- and nanometer-scale mechanical elements, sensors, actuators, and electronic circuits on one carrier or even on one chip. This entry was prepared in the late 1970s, for instance with the demonstration of a batch-fabricated silicon accelerometer with piezoresistive transducers. The silicon bulk micromachined proof mass was bonded between two glass wafers [Roylance and Angell 1979]. The commercialization of similar devices began around 10 years later and was very soon based on a variety of available transducer principles such as the sensing of capacitance changes between fixed and movable plates, the frequency measurement of resonant devices, the stabilization of a tunneling current by a closed-loop system, the sensing of thermal changes between a heater and a movable heat sink, and the sensing of changes of the thermal distribution within an air bubble. This broad invasion of new and old ideas in the world of micro-electronic technologies has opened the way to inexpensive mass applications of inertial sensors in industry, cars, medicine, consumer goods, and so on.

Everybody knows the pioneering role of MEMS-based 50g accelerometers used in airbag ignition devices, which became the first high-volume product in the area of inertial MEMS. It was especially encouraging that within these successful high-volume products an example of the full monolithic integration of sensor and

signal processing on one chip could be found. Analog Devices, supported by strong governmental funding, developed a special BiCMOS-MEMS process combining a known microelectronic process with a polysilicon deposition, etching, and release technology. Various inertial sensors were developed on the basis of this process, of which the first was the 50g accelerometer [Analog Devices 1993].

### *Gyroscopes*

The stabilizing effect of rapidly rotating disks has been known for a long time and was used in ancient times for yo-yo-like toys and for ceremonies. Real angular-rate sensors emerged quite late but have had a remarkably long history compared with accelerometers. This obviously is due to the much lower early requirements on the speed of the interfaces and, of course, to the moderate values of the signals to be measured. For instance, the Earth's rotation is characterized by a rate signal of  $360^\circ/24$  hours or  $0.1^\circ/s$ .

The first technical realization of an angular-rate sensor took place around 1817 with the mechanical gyroscope designed by Johann Gottfried Friedrich von Bohnenberger in Tübingen in Germany. It was not a true sensor but a demonstrator of rotational effects.

The system was based on the spinning top and – not surprisingly – was used to demonstrate the mechanism of the Earth's axis' very slow precession accelerated in duration from a full cycle of 25 800 years to a small amount of seconds or minutes. Similar demonstrators were built around 1830 by the American Walter Johnson (Johnson's Rotascope).

The principle underlying the emergence of Coriolis forces within a rotating non-inertial coordinate system was demonstrated in 1851 by the French scientist Leon Foucault by building a 67-m-long pendulum with a mass of 28 kg within the Paris Pantheon (Fig. 1.1). This was the first real rotation sensor which measured the rotation of the Earth. Incidentally, a similar experiment was first performed in 1661 by the Italian physicist Vincenzo Viviani and, after Foucault, implemented in countries all over the world. Under the influence of the Earth's rotation the oscillation plane of such a pendulum changes by  $360^\circ \sin \varphi$  in 24 hours. The angle  $\varphi$  is the geographic latitude of the experimental location. At the equator, the Foucault Pendulum does not show any reaction; at the poles, the rotation would be the full  $360^\circ/24$  hours. At all other places the tip of the pendulum will draw nice rosettes on the floor.

The Coriolis force was introduced by Gaspard-Gustave Coriolis, a French scientist, who described it in 1835. The Coriolis force appears in the equation of motion of an object in a rotating frame of reference and depends on the linear or angular velocity of the moving object. It will be considered in more detail in Chapter 8.

Using this principle, in 1852 Foucault built a spinning-top gyroscope (“*Meridiankreisel*”), which can be considered the basis of modern spinning-top gyros. The term “gyroscope” was introduced at this time (“gyros” – rotation, “skopein” – vision). However, the rise of rotation sensors was preceded by the use

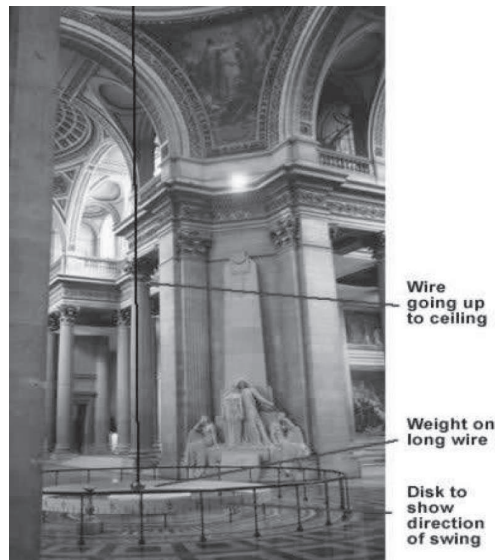


**Figure 1.1** Foucault's Pendulum, in the Pantheon, Paris.

of the stabilizing ability of spinning wheels in torpedoes and cannon ammunition. Only in 1904 was the technical principle of the fast-spinning-top gyroscope patented by the German art historian Hermann Anschütz-Kämpfe [Schell 2005], who developed the idea of using the gyroscope within a compass (in 1908). The spinning wheel in a gyroscope is mounted on gimbals so that the wheel's axis is free to orient itself. The key element for a compass was the introduction of a mechanism that results in an applied torque whenever the compass' axis is not pointing North. The precession returns the compass' axis towards the true North if it is disturbed towards another orientation.

Other inventors such as the American Elmer Ambrose Sperry (1910) followed Anschütz-Kämpfe, and the acceptance of the gyro-compasses by the navy led to a quick penetration first on large ships and later on smaller ones and on airplanes.

Inertial navigation and platform stabilization in aircraft and naval vessels remained the domain of spinning-top gyroscopes for a very long time. Driven by the requirements for cost reduction and miniaturization, around 1960 new types of gyros like the vibrating-string gyro [Quick 1964], the tuning-fork gyro [Hunt and Hobbs 1964] and the vibrating-shell resonator emerged and opened the way to a drastic size and weight reduction, which finally ended with the transfer of these principles into the world of MEMS. The vibrating-string principle is based on the action of the Coriolis force on a simple oscillator such as a mass on a string or a vibrating beam; the tuning-fork principle is based on balanced oscillators; and the vibrating shell uses the two vibration modes of a ring or a cylinder as in the classic wineglass effect. These principles will be presented in Chapter 8.

The new miniaturized vibrating gyros captured marked shares of the market step by step. However, for high-precision applications a rival for the classical gyros emerged around the end of the 1970s: the optical gyroscope. These gyros based on optical ring resonators and later on fiber optics have dominated, for instance, the aircraft navigator market since 1980.

The transition from miniaturized gyros to the MEMS gyros was smooth. In miniaturized gyros it has become more and more difficult to realize bearings for endlessly rotating objects. The same problem applies for the early MEMS technologies and – with respect to specific friction, wear, and reliability – is still present today despite all the progress in this area. Only in 2008 did the first rotating MEMS gyro, developed by the Japanese company Tokimec, emerge on the market. Previous MEMS gyros used not the spinning-top principle, but rather the vibration or oscillation of masses within small linear or angular intervals as prepared by the miniaturized mechanical constructions. These so-called Coriolis vibratory gyroscopes (CVGs) – irrespective of whether or not they are based on MEMS – use at least two vibration modes of the structure, in which the Coriolis force excited by the interaction of the external rotation with the so-called primary mode causes an energy transfer to the secondary vibration mode. The vibrating elements are joined to hinges or anchors via springs. Such springs can be outstandingly formed in silicon because silicon possesses not only excellent mechanical and thermal properties in comparison with classical metals but also outstanding machinability.

However, the full implementation of a complete gyroscope structure by using only microelectronic or emerging MEMS technologies was not the first step towards MEMS-based gyroscopes. Instead the designers first tried to use MEMS technologies to create key components for miniaturized gyros, such as the quartz tuning forks with piezoelectric actuators and piezoresistive transducers developed by Systron Donner [Soderkvist 1990] and the silicon-based rings including the spring suspension for the vibrating-shell systems developed by British Aerospace System and Equipment [Hopkin 1997]. Such components were then mounted on appropriate carriers. Concurrently, typical MEMS-technology-based devices formed and bonded on wafer level were proposed around 1986 by the Charles Draper Laboratory [Greiff *et al.* 1991] and demonstrated first in 1991 with a bulk-micromachined tuning-fork gyroscope and a little bit later, in 1993, with a silicon-on-glass tuning-fork gyroscope [Weinberg *et al.* 1994]. In 1998, researchers at the University of Michigan demonstrated a polysilicon-ring gyroscope produced with a trench-refill technology [Ayazi and Najafi 1998]. Predecessors of different batch-fabricated gyros that used more exotic technology exist, but these designs could not prevail against products based on technologies that were becoming mainstream MEMS technologies. One of the most interesting of the non-mainstream products was the vibrating-ring gyroscope of the University of Michigan produced using metal electroforming of nickel into a thick polyimide mold on a silicon substrate, which was demonstrated in 1994 [Putty and Najafi 1994].

There were hundreds of different demonstrators from the University of Berkeley, from Samsung and Murata, from the Hahn-Schickard Gesellschaft-IMIT (Germany) and many others, but only a few were commercially successful. An excellent overview of the emerging MEMS-based inertial sensors can be found in Yazdi *et al.* [1998], which can be complemented by reading Shkel [2001].

## 1.2 Applications and market

The applications of the classical accelerometers are vibrometry, shock detection, tilt measurement, dynamometry, seismology and other areas related to test and evaluation of devices exposed to inertial forces. Some of these applications coincide with the main application areas of classical gyroscopes – inertial navigation and platform stabilization. MEMS technologies dramatically changed this relatively peaceful picture. Nearly every month a new application is created and checked for commercial attractiveness and realizability.

### *Some general trends*

The trends of the inertial-MEMS market's development are not significantly different from those of the entire MEMS market if one excludes the two leading and very old and stable products – ink-jet heads for printers and write/read heads for magnetic and optical memory disks. These two market segments alone occupied around an estimated 25% of the about 10 Bn \$ MEMS market in 2010. MEMS addressed very fragmented markets that have had predominantly low-volume and only a few large to truly high-volume applications. This market is transforming more and more into a high-volume market with steadily expanding size, and, crucially, with a growing number of different applications.

Compound annual growth rates (CAGRs) of 5% to 20% are typical for these different applications. At present the number of companies manufacturing MEMS products is around 270 in addition to 150 fab-less companies. Around 90 R&D industrial facilities, which are able to develop prototypes and to perform small-volume production, round off the picture of today's MEMS community. It should be borne in mind that in the 1990s three to five years were needed to develop new MEMS designs and five to eight years from the prototypes to volume production. In the case of safety-critical applications the time lapse was even longer. Now the overall time from design start to volume production has decreased by a factor of two to three and is reducing further. Consequently, the interest in research and development is enormous and is still growing. It will continue to grow as long as MEMS products penetrate all areas of human activity. Today the distance which has thus far been covered on the way to all-encompassing applications of MEMS and inertial sensors is almost negligible in comparison with the distance still to go.

*The inertial-MEMS market*

Within the MEMS market modern inertial sensors – accelerometers and gyros – have gained a considerable share, exceeding 20% of the expected 12 Bn \$ MEMS market in 2011 (~6 Bn \$ in 2009). In 2005 nearly 80% of all applications were related to automotive safety functions such as automatic break systems (ABSs), airbag sensors, rollover sensors, electronic stabilization systems (ESP), and other anti-skid systems as well as to navigation. Starting with 50g accelerometers in airbag safety systems, the next step – the introduction of electronic stabilization control (ESC) by Bosch and Systron Donner in 1994 – was significantly accelerated by the disastrous elk test of the newly invented Mercedes-Benz A-Class in 1997. ESC had to rescue the reputation of the brand name of one of the leading makers of high-quality cars. In ESC, yaw-rate gyroscopes and low-g sensors are usually the decisive information sources for controlling the finely allotted brake forces on the different wheels to avoid accidents.

Rollover protection, highly sophisticated front and side airbags combined with safety-belt control, and suspension control, especially for trucks, and many other applications have not only expanded the market but also forced the development of new low-g accelerometers, of gyroscopes sensitive in different axes and with different accuracy levels, and – importantly – the co-integration of two or more sensors in one package or even on one chip.

Remarkably, the market shares of gyroscopes and accelerometers nearly equalized around 2005. New accelerometer applications mainly in the consumer market have shifted the relation to a stable 40% share of gyroscopes within the inertial-MEMS market. After 2012–13 the picture may change because the killer applications in the consumer market, which with an expected 1 Bn \$ contribution will then be at least comparable in size to the other segments, have not yet been defined and are hard to predict.

Today, large companies are fighting for their share in the market of automotive inertial MEMS sensors. Among these, the world's largest MEMS-sensor manufacturer is Bosch in Germany, which has put considerable effort into the production of MEMS gyroscopes for automotive applications. However, British Aerospace Equipment Silicon Sensor Systems (BAE SSS), BEI Systron Donner, Delphi-Delco, Murata, Matsushita, and Samsung have also long been very successful and delivered many millions of gyros to component manufacturers in the car industry. Within the accelerometer market the Norwegian company Sensoror, with its 50g accelerometers, and the Swedish VTI Technologies, which was long the leader in the low-g accelerometer market, have made surprisingly dominant contributions to the emerging killer applications within the automotive industry. However, the number of high-volume players in the inertial sensor market is quite limited, encompassing Bosch, Analog Devices, Freescale, and almost a dozen others.

Besides the automotive industry, the remainder of the market is dictated by consumer applications, which in recent years have shown dramatic growth, with CAGR 25%–30%. Accepted and growing applications are related to the use of

inertial sensors in hand-held cameras for picture stabilization, in personal computers for hard-disk protection against mechanical shocks, in pedometers for motion sensing, and in more exotic products such as the two-wheel Human Transporter of Segway. Probably one of the most interesting applications is the motion sensing integrated into mobile phones, game controllers, toys and other human-machine interfaces. The Nintendo Wii's motion-sensing remote control has attracted the broad interest of the public to inertial MEMS. The consumer and information technology (IT) sector has increased from about 10% in 2005 to about a 45% share in 2009/10.

Within the consumer market the companies Analog Devices, Kionix, ST Microelectronics, and MEMSIC are the dominating players within the accelerometer business, while Panasonic and Murata have long led the gyro market. However, every year new companies are entering the market for inertial sensors, and the established manufacturers of inertial MEMS as well as newcomers are focusing their attention more and more on the consumer market. New systems such as very small and cheap one-axis sensors as well as more highly integrated multi-dimensional accelerometers and gyroscopes are now on the market. ST Microelectronics introduced in 2009 a three-axis high-performance gyroscope, whereas VTI announced a three-dimensional (3D) accelerometer combined with a 1D gyroscope [[MEMSentry 2009](#)]. Sensordynamics introduced in 2008 a combined one-axis accelerometer and one-axis gyroscope [[Micronews 2009](#)] and announced a three-axis accelerometer plus one-axis gyro combination. The race into the world of multi-axis inertial sensors, including completely integrated (six-axis) inertial measurement units (IMUs), is fully under way.

An IMU measures the accelerations and rotation rates on all three axes and, in principle, represents the (functionally) ultimate inertial sensor. Applications are numerous, ranging from medical 3D gesture and motion recognition via human-machine interfaces (HMIs) for game controllers and mobile phones to personal navigation systems.

The high-volume application of inertial MEMS in the automotive and consumer markets was for a long time in some contrast with aeronautic and defense applications. Here the high added value guaranteed a large benefit for the customer, and, consequently, the low quantities have been to some extent compensated for by good prices. Remarkably, within the last few years many inertial-MEMS products developed for the aeronautic and defense sector have reached commercialization. This sector has doubled within the last five years, approaching now around 50% of the size of the automotive segment.

As with aeronautics and defense markets, the industrial and medical segments of inertial MEMS' applications are also at the stage of entry to high-volume markets. Applications such as activity monitoring in pacemakers have considerable dissemination throughout the world. It can be expected that the inertial control of robots and machine parts with more than one degree of freedom (DOF) will achieve a quite broad distribution.

## 1.3 The ingredients of inertial MEMS

Inertial sensors convert the inertial forces caused by the input acceleration or rate signal into some physical changes such as deflection of masses or deviations of stresses, which then are captured by a corresponding transducer and transformed into an electrical signal. The electrical signal is subjected to some estimation procedures such as linear or nonlinear filtering in order to derive an estimate of the input signal. The final output represents the calibrated value of the measured acceleration or rate. Of course, not only electrical output signals are feasible; however, only in such exceptional cases as for instance in highly explosive environments are other forms of the output, such as optical signals, used. Within this book only sensors with electrical output signals are treated.

Accelerations and angular velocities are vectorial signals possessing absolute values and orientations. If only one component of the vector should be measured the sensor is denoted 1D or one-axis. If two or all three components of the acceleration or the rate signal should be captured, the sensor is called a 2D or 3D accelerometer, or a rate sensor.

Today a MEMS-based accelerometer or gyroscope is understood as a complete product that is packaged, calibrated, and tested, and has to be delivered to the customer, who wants to integrate this component with minimal effort into a higher-level measurement or control system. The level of accuracy required depends on the application. The environmental conditions for the integration of inertial MEMS at the customer site may be also quite different and usually are divided into classes with respect to the applicable temperature range and the exposure to humidity and aggressive chemicals as well as to vibration and shocks. The length of the lifetime, the reliability, and the safety against failures during operation may vary significantly, and to a large extent determine the product's price. Consequently, orders of magnitude may separate the complexity and the price of an inertial MEMS for different applications even if the underlying sensor principles are identical.

In order to make the following explanations and terminology systematic, it is meaningful to sketch a general structure of a sensor system with emphasis on inertial sensors. The system consists of not only the sensor itself but also additional components such as transducers and electronics. In Fig. 1.2 a very crude representation of the whole system is shown. The intrinsic sensor transforms the input signal – acceleration or rate – into a physical objective, which can be gathered by the transducer and transformed into an electrical signal. The sensor and transducer are subject to interactions with the package. In inertial MEMS the main interactions are stress and heat transfer. Environmental factors may be transferred via the package to the sensor and transducer, changing their behavior.

The electronic part consists of an input stage that amplifies the transformed signal into a conveniently manageable form. The electronics also may generate

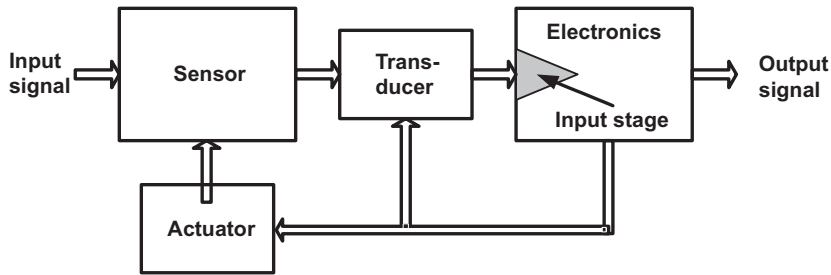


**Figure 1.2** The general architecture of a sensor system.

excitation and control signals that are necessary for bias setting and for operational conditioning. Actuating stimuli may be used, for instance, for feedback control, as well as for test signals. In practice the borders between these generic blocks are quite fuzzy. The transducer and the electronic input stage often form an indivisible object where the input stage provides the necessary biasing and excitation for the transducer and, vice versa, parts of the input stage may act as components of the transducer. The transducer is often directly integrated into the intrinsic sensor. In general, the application of a certain transducer principle usually entails not only the choice of a certain transducer element but also the adaption of the sensor and the electronics.

Nevertheless, the generic structure shown allows us to systematize the understanding of the main interactions between the components.

- Feedback control is beneficial with respect to linearity and optimization of transfer characteristics. However, it requires actuators and, thus, additional effort. Therefore, not all sensors have feedback components and, where possible, sensors operate in an open-loop mode.
- The system performance is to a large extent determined by noise and disturbances. Typical noise sources exist within inertial MEMS. So, the intrinsic inertial sensor exhibits mechanical noise caused mainly by friction with the usually gaseous environment. For not-too-ambitious performance targets the dominant noise stems from the second noise source – the transducer and electronic stages, and here mainly from the electronic input stage.

In accord with the system structure illustrated, the various basic sensor principles, the transducer mechanisms, the corresponding governing models, and, last but not least, the typical error sources and performance parameters of the overall system will be covered by this book.

The seemingly central role of the sensor principle within inertial MEMS quickly dissolves when one looks at the many stages of creating the final product.

- A working environment for the sensor is usually established by the so-called zero-level packaging.
- The sensor signals must be acquired and processed.

- In many cases, as for instance in all vibratory gyroscopes, the sensor has to be driven in a primary movement that must be controlled to high accuracy.
- For high-performance applications, on-line-monitoring functions are integrated.
- The output signals for the external communication – including, if applicable, the results of in-built tests – and monitoring must be formed.
- The sensor and the signal-processing unit have to be packaged and bonded to connections with the external pins or solder balls of the (first-level) package.
- The whole product must be calibrated, which requires special equipment in order to create the necessary accelerations or rate signals with high accuracy. Selected representative functions are tested, usually within the entire temperature range of application.
- Last but not least, more or less comprehensive qualification procedures must be passed before production may be initiated.

Similarly to most other MEMS applications, the key for success within the area of inertial MEMS is the comprehensive development and integration of all the mentioned components necessary for these multidisciplinary products: MEMS technologies, first- and second-level packaging, application analysis, system design considering the specific effects of technology tolerances and forces in a micro- to nano-scale environment, test methods for high-volume production, and, finally, reliability and lifetime guarantees on an unprecedented scale, especially for automotive and medical applications.

Huge investments were necessary to build up high-volume fabs and to run a high-yield production. Partial solutions have reached some maturity. For instance, selected surface and bulk micromachining technologies of leading manufacturers and of R&D facilities have become something like standard processes and are free to be used by the scientific community for prototype development. However, most of the subareas are still in a phase of rapid growth and improvement. Correspondingly, product cycles are changing rather quickly despite the stringent stability requirements of the automotive industry. The third generation of acceleration sensors and gyroscopes is now on the market, the next generation *ante portas*.

## References

- Analog Devices (1993). ADXL50 – monolithic accelerometer with signal conditioning. Data sheet, Analog Devices, Norwood, MA.
- Ayazi, F. and Najafi, K. (1998). Design and fabrication of a high performance polysilicon vibrating ring gyroscope, in *Proceedings of the IEEE Micro Electro Mechanical Systems Workshop (MEMS '98)*, Heidelberg, pp. 621–626.
- Greiff, P., Boxenhorn, B., King, T., and Niles, L. (1991). Silicon monolithic micromechanical gyroscope, in *Proceedings of the IEEE 1991 International*

- Conference on Solid State Sensors and Actuators*, San Francisco, pp. 966–968.
- Hopkin, I. (1997). Performance and design of a silicon micromachined gyro, in *Proceedings of the Symposium on Gyro Technology*, Stuttgart, pp. 1.0–1.10.
- Hunt, G. W. and Hobbs, A. E. W. (1964). Development of an accurate tuning-fork gyroscope, in *Symposium on Gyros, Proceedings of the Institute of Mechanical Engineers (London), 1964–65*, **179**(3 E).
- McCullom, B. and Peters, O. (1924). A new electric telemeter. *Technology Papers of the National Bureau of Standards*, **17**(247).
- MEMSentry (2009). ST’s new 3-axis analog gyroscope. *MEMSentry*, December 2009, **47**:5.
- Micronews (2009). Inside the first combination inertial sensor. *Micronews*, May 2009, **80**:7.
- Putty, M. and Najafi, K. (1994). A micromachined vibrating ring gyroscope, in *Technical Digest Solid-State Sensor Actuator Workshop*, Hilton Head Island, SC, pp. 213–220.
- Quick, W. H. (1964). Theory of the vibrating string as an angular motion sensor. *Transactions of the ASME Journal of Applied Mechanics*, 523–534.
- Roylance, L. M. and Angell, J. A. (1979). A batch-fabricated silicon accelerometer. *IEEE Trans. Electron Devices*, **26**:1911–1917.
- Schell, B. (2005). 100 Years of Anschuetz gyro compasses – 100 years of innovations in nautical technology, in *Symposium Gyro Technology 2005*, Stuttgart, pp. 1–20.
- Shkel, A. M. (2001). Micromachined gyroscopes: challenges, design solutions, and opportunities. *Proceedings of the SPIE*, **4334**:74–85.
- Soderkvist, J. (1990). Design of solid-state gyroscopic sensor made of quartz. *Sensors and Actuators A*, **21/23**:293–296.
- Weinberg, M., Bernstein, J., Cho, S. *et al.* (1994). A micromachined comb-drive tuning fork gyroscope for commercial applications. *Proceedings of the Sensor Expo*, Cleveland, OH, pp. 187–193.
- Yazdi, N., Ayazy, F., and Najafi, K. (1998). Micromachined inertial sensors. *Proceedings of the IEEE*, **86**(8):1640–1659.

# 2 Transducers

---

The basic building blocks of inertial MEMS are sensing elements to acquire the reaction of the measurement system, actuators to excite the mechanical system, and other components of the mechanical system such as proof masses, beams, springs, and suspensions. The properties and dimensions of all these components are decisive for their application within a given sensor system.

Silicon, with its outstanding mechanical properties (e.g. [Gad-el-Hak \[2002\]](#) and [Franssila \[2004\]](#)), plays a key role for building these blocks. It is as strong as steel. It is ideally elastic, not exhibiting plastic deformations up to the yield point as do most metals. The elastic modulus  $E$  may be as large as 190 GPa, depending on crystal orientation, and the yield strength is about 7 GPa. With appropriate doping (boron, phosphorus) concentration the resistivity can be changed by eight orders of magnitude between  $10^{-4}$  and  $10^4 \Omega \text{ cm}$ ; thus structures such as conductive plates or comb fingers can be manufactured. The density of silicon is  $2300 \text{ kg/m}^3$ , the thermal conductivity is  $1.57 \text{ W/(cm K)}$ , and the thermal expansion coefficient  $CT = 2.33 \times 10^{-6}/\text{K}$  [[Kovacs 1998](#)].

Polycrystalline silicon, or “polysilicon” for short, which is made up of small single-crystal domains of silicon (grains), has similar properties and is the most popular building material for surface-micromachined devices (SMMs).

Monocrystalline silicon is anisotropic and exhibits pronounced orientation-dependent properties such as piezoresistivity and piezo-Hall effects. The mechanical and electrical properties of polysilicon are slightly inferior to those of monocrystalline silicon but are very similar to those of an isotropic material; thus, the material is much easier to handle than monocrystalline silicon.

While the main focus of this chapter is on transducers, some material properties that are relevant to both transducers and general mechanical components of inertial MEMS will be summed up first in order to better understand the relevant transducer mechanisms.

## 2.1 Anisotropic material properties, tensors, and rotations

Anisotropic material properties play a prominent role in inertial MEMS. A suitable mathematical description of these properties is provided by the concepts of stress and strain. Considering the fundamental role of these terms in the

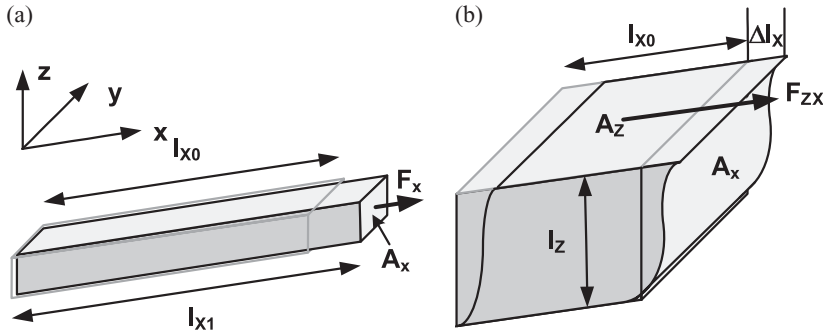


**Figure 2.1** Axial and shear forces acting on a body. (a) Beam elongation under axial force. (b) Cube deformation under shear load.

engineering literature, a short introduction to the matter is given. Readers familiar with these concepts can skip this section.

### 2.1.1 Stress, strain, and piezoresistivity

#### Hooke's law

The concept of stress and strain was developed in order to describe the interrelation between external forces, acting on a solid body, and the internal forces between the volume elements of the body, which cause the deformations. Another objective was to reflect the effects a strained condition can induce on material properties such as resistivity.

Stress is a force distribution and strain is the distribution of deformations.

#### Normal stresses

The stress–strain relation is a generalization of Hooke's law, which, when applied to a metal bar orientated along the  $x$ -axis and with length  $l_{x0}$  and cross-section  $A_x$ , can be expressed as (see Fig. 2.1(a)):

$$F_x = EA_x \frac{\Delta l_x}{l_{x0}} \quad \text{or} \quad \sigma_x = E\varepsilon_x, \quad (2.1)$$

where  $\sigma_x$  is the axial stress, i.e. the applied axial force per unit area that is normal to the surface,

$$\sigma_x = \frac{F_x}{A_x}, \quad (2.2)$$

and  $\varepsilon_x$  is the (normal) strain, i.e. the dimensionless relative elongation

$$\varepsilon_x = \frac{l_{x1} - l_{x0}}{l_{x0}} = \frac{\Delta l_x}{l_{x0}}. \quad (2.3)$$

$E$  is the elastic modulus or Young modulus of the given material. It expresses the material's resistance to elastic deformations. A large elastic modulus characterizes a stiff material and a small  $E$  characterizes a highly elastic object. If

the applied forces cause an elongation of the object, the resulting stress is called tensile; in the opposite case the stress is called compressive.

For ordinary materials, the elongation of the bar is accompanied by a reduction of its lateral dimensions (contraction of the bar), i.e. by a transverse strain

$$\varepsilon_{yy} = \varepsilon_{zz} = \frac{\Delta l_y}{l_y} = \frac{\Delta l_z}{l_z}. \quad (2.4)$$

The ratio of the lateral to the axial strain  $\varepsilon_t/\varepsilon_a$  is Poisson's ratio

$$\nu = -\frac{\varepsilon_{zz}}{\varepsilon_x} = -\frac{\varepsilon_{yy}}{\varepsilon_x}. \quad (2.5)$$

Within the elastic range of the medium,  $\nu$  is constant, and for most materials its value is between 0.2 and 0.35. An upper limit of 0.5 exists and pertains to ideally incompressible media. For an isotropic elastic object, which is subject to applied stresses along all three orthogonal axes, the strain in any of the three directions is the sum of the elongation in that direction minus the contraction caused by the stresses in the two remaining orthogonal axes, for instance

$$\begin{aligned} \varepsilon_x &= \frac{1}{E}[\sigma_x - \nu(\sigma_y + \sigma_z)]; & \sigma_x &= \frac{E}{(1+\nu)(1-2\nu)}[(1-\nu)\varepsilon_x + \nu(\varepsilon_y + \varepsilon_z)], \\ \varepsilon_y &= \frac{1}{E}[\sigma_y - \nu(\sigma_x + \sigma_z)]; & \sigma_y &= \frac{E}{(1+\nu)(1-2\nu)}[(1-\nu)\varepsilon_y + \nu(\varepsilon_x + \varepsilon_z)], \\ \varepsilon_z &= \frac{1}{E}[\sigma_z - \nu(\sigma_x + \sigma_y)]; & \sigma_z &= \frac{E}{(1+\nu)(1-2\nu)}[(1-\nu)\varepsilon_z + \nu(\varepsilon_x + \varepsilon_y)]. \end{aligned} \quad (2.6)$$

On the right-hand side the equation is resolved for the case in which the strains are known.

For "non-standard" materials such as foams and synthetic compounds Poisson's ratio can take negative values; however, such materials are not considered in this book.

### Shear stresses

Besides the normal stresses, which are perpendicular to the body's surfaces, shear stresses exist, particularly in twisted bodies. A shear force acts parallel to a given surface as shown in Fig. 2.1(b). For instance,  $F_{zx}$  denotes a force in the  $x$ -direction acting parallel to a surface whose normal vector is oriented along the  $z$ -direction. The shear stress is the shear force per unit area. Shear forces create shear strain, i.e. deformations along the direction of the shear force. In Fig. 2.1(b) the shear strain  $\varepsilon_{zx}$  is the ratio between the displacement  $\Delta l_x$  and the height of the cube  $l_z$ . Shear stress and shear strain are related to each other by the shear modulus  $G$ :

$$F_{zx} = GA_z \frac{\Delta l_x}{l_z} \quad \text{or} \quad \sigma_{zx} = G\varepsilon_{zx}. \quad (2.7)$$

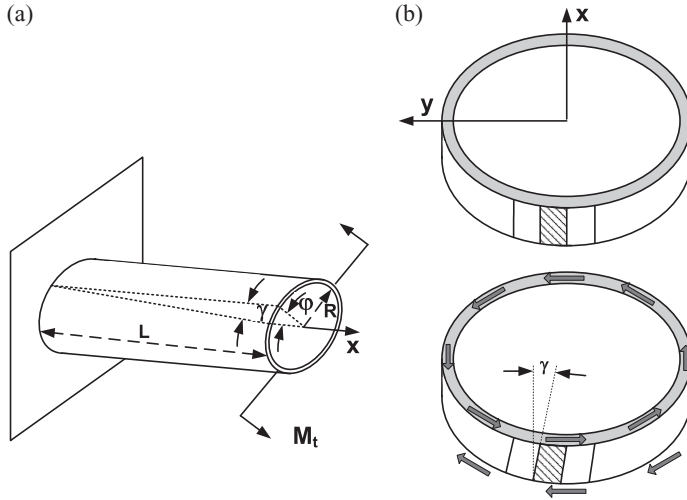


**Figure 2.2** Torsion of a hollow cylinder. (a) A twisted cylinder. (b) Cross-sections of untwisted and twisted hollow cylinders.

The basic experiment to determine the relation between shear stress and shear strain is shown in Fig. 2.2(a). A homogeneous hollow cylinder with thin walls is exposed to a torsional moment at both sides, and the resulting shear angle  $\gamma$  is measured. This angle determines the torsion or twist angle  $\varphi$  of the front face of the cylinder according to the obvious relation

$$\varphi = \gamma \frac{L}{R}, \quad (2.8)$$

where  $L$  is the length of the cylinder,  $t$  is the thickness of the wall, and  $R$  is the radius of the cylinder. Assuming that the stress across the cross-section of the cylinder,  $\sigma_t$ , which is orientated in the tangential direction, is constant, the moment created is  $R\sigma_t A$ , where  $A$  is the area of the cross-section. This moment is balanced by the applied  $M_t$ ,

$$M_t = 2\pi R^2 t \sigma_t. \quad (2.9)$$

By measuring  $M_t$  and the shear angle  $\gamma$ , the ratio  $\sigma_t/\gamma$  can be determined. Within the limits of elastic deformation without warping it has been found that

$$\sigma_t = G\gamma. \quad (2.10)$$

The shear angle  $\gamma$  is the deformation angle of the elementary rectangles of the cylinder as shown in Fig. 2.2(b). For the marked rectangle (in the middle of the bottom part of the cylinder) the stress lies in the plane  $x = \text{constant}$  and is directed along the  $y$ -axis:  $\sigma_t = \sigma_{xy}$ .<sup>1</sup> The shear angle  $\gamma$  is exactly double the shear strain  $\gamma = 2\varepsilon_{xy}$ . Using this definition and applying the results to an arbitrary

<sup>1</sup> The natural coordinate system is here a cylindrical system in which  $\sigma_t = \sigma_{x,\varphi}$ .

volume element of an isotropic body, the shear stress–strain relation can be written in the more common notation

$$\varepsilon_{xy} = \frac{\sigma_{xy}}{2G}; \quad \varepsilon_{xz} = \frac{\sigma_{xz}}{2G}; \quad \varepsilon_{yz} = \frac{\sigma_{yz}}{2G}, \quad (2.11)$$

which together with Eq. (2.6) represents the generalized form of Hooke’s law. It is valid for small deformations, where the superposition principle remains in force, i.e. the resulting deformation caused by different forces can be substituted by the sum of the deformations caused by these forces.

A deeper insight into the fundamentals of the theory of elasticity reveals that for isotropic materials the original tension test of Hooke without any additional torsion test is sufficient to derive not only the deformations caused by normal stresses, but also the relation between shear forces and corresponding deformations. This leads to a well-defined interrelation between Young and shear moduli presented below (Eq. (2.36)).

However, the torsion test is illustrative with respect to torsional components of inertial springs and allows us to introduce the basic ideas for the analysis of torsional springs.

## Stress and strain tensors

Usually, objects subject to external forces are not built as simply as the ones considered so far, i.e. bars or torsional cylinders. They may have a complicated geometry and may be exposed to a combination of normal and shear stresses. To analyze the reaction of the body, the external forces have to be related to the internal forces and deformations at different inner points. Consequently, the concepts of stress and strain must be brought down to infinitesimal length scales, where balance of force and momentum is applied on each face of such an entity. On the basis of such a representation, partial differential equations for the relation among stress, strain, and global and local forces within the body can be derived; as usual, they must be complemented by appropriate boundary conditions. These equations can be numerically simulated or – in some exceptional cases – solved analytically.

### *The stress tensor*

To derive an infinitesimal description of the stress or strain distribution, infinitesimal volume elements of the medium, pertaining to a Cartesian coordinate frame, are considered; for such coordinates, the volume elements are cubes, as can be seen in Fig. 2.3 [Popov 1968, 1999], The faces of the cube have areas  $dA$ . The medium is supposed to be in a state of mechanical equilibrium; this implies that forces and moments either originating from interaction with neighboring volume elements or being imparted by external sources must be balanced at each face of each volume element. At the boundary of the body, external load forces and reaction forces of the supports have to be added.

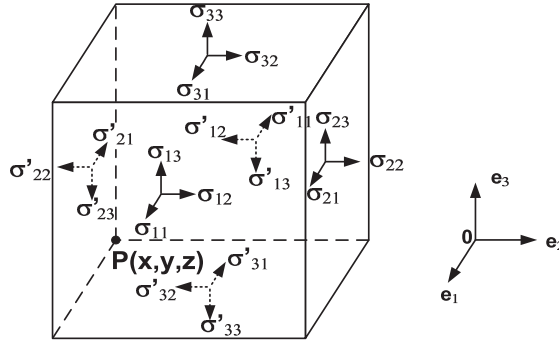


**Figure 2.3** The stress tensor.

For convenience the  $x$ -,  $y$ -, and  $z$ -axes are often defined by the vectors  $\bar{e}_1, \bar{e}_2$ , and  $\bar{e}_3$ , and the corresponding coordinates are

$$x \Rightarrow x_1, \quad y \Rightarrow x_2, \quad z \Rightarrow x_3. \quad (2.12)$$

A force or a stress component acting on the face with normal vector  $\bar{e}_i$  and oriented along direction  $\bar{e}_j$  is termed  $\Delta F_{ij}$ . The stress is the limit  $\sigma_{ij} = \Delta F_{ij}/dA_i|_{dA_i \rightarrow 0}$ . The cube under consideration is in mechanical equilibrium with adjacent cubes so that the total force exerted on a face of the cube is compensated for by the corresponding force of the adjacent cube. The stress at a face  $\bar{\sigma}_i = \Delta \bar{F}_i/dA$  is decomposed into the orthogonal components  $\sigma_{ii}$ ,  $\sigma_{ij}$ , and  $\sigma_{ik}$ . The normal stress  $\sigma_{ii}$  is caused by the force perpendicular to the face and tends to compress or elongate the cube. Shear stresses act parallel to the face and tend to shift the corner points of the face, thus distorting the cube into a rhomboid. Mechanical equilibrium implies that the total force and the total torque acting on the cube must be zero. This has two implications.

1. The normal stresses at opposite faces have the same values but opposite directions  $\sigma'_{ii} = -\sigma_{ii}$ .
2. Zero total torque about any axis requires that the stress components must satisfy a symmetry condition,

$$\sigma_{ij} = \sigma_{ji}. \quad (2.13)$$

Stress components at opposite faces have opposite orientations by definition. A complete description of the state of stress at point  $P(x, y, z)$  is then given by nine quantities  $\sigma_{ij}(x, y, z)$ , and is subject to the symmetry condition (2.13), which reduces the number of independent quantities to six. This collection of quantities  $\sigma_{ij}(x, y, z)$  at  $P(x, y, z)$  defines the coordinates of the so-called stress tensor at  $P(x, y, z)$ . The stress tensor represented within the given coordinate system can be represented by the coordinate matrix  $\sigma$  with nine components

**Table 2.1.** Index transfer by Voigt's notation

Matrix indices	11	22	33	23, 32	13, 31	12, 21
Vector index	1	2	3	4	5	6

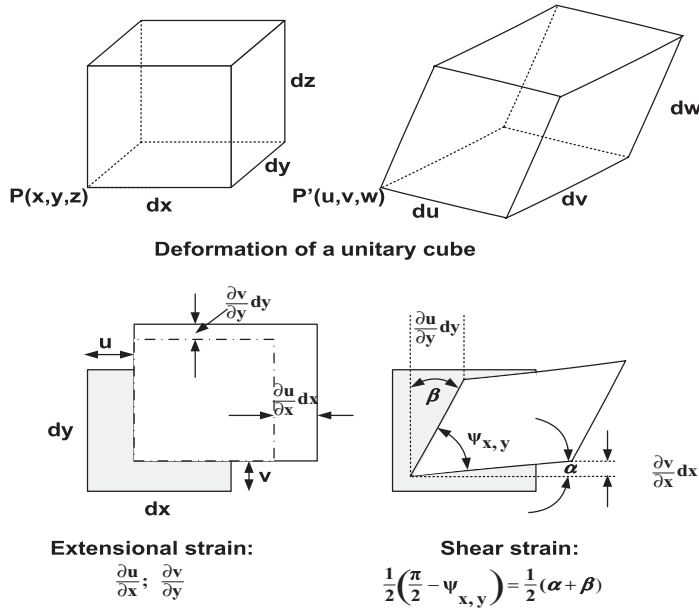


**Figure 2.4** Deformation of an elementary cube.

$\sigma_{ij}; i, j = 1, 2, 3:$

$$\sigma = \{\sigma_{ij}\}. \tag{2.14}$$

In this book, tensor quantities are usually represented in a given coordinate system. As a consequence, matrix algebra can be used to express tensor relations.

Since the symmetry property (2.13) reduces the number of independent stress components from nine to six, it is convenient to express the stress status not by a  $3 \times 3$  stress matrix but by a stress vector  $\bar{\sigma}$  using Voigt's notation, which is based on the equivalence of indices (shown in Table 2.1):

$$\bar{\sigma}^T = (\sigma_1 = \sigma_{11}, \sigma_2 = \sigma_{22}, \sigma_3 = \sigma_{33}, \sigma_4 = \sigma_{23}, \sigma_5 = \sigma_{13}, \sigma_6 = \sigma_{12}). \tag{2.15}$$

The superscript T denotes the transpose of a vector or a matrix.

*The strain tensor*

The strain tensor can be introduced in the same way as the stress tensor. Again, a non-deformed cube is considered at point  $P(x, y, z)$  (see Fig. 2.4). The deformation of the cube is described by the displacements each of its corner points

is undergoing. Thus, a point with coordinates  $(x, y, z)$  in the undeformed state will take the location  $(u(x, y, z), v(x, y, z), w(x, y, z))$  after deformation. A point  $(x + \Delta x, y + \Delta y, z + \Delta z)$  nearby will move to

$$\begin{aligned} \begin{pmatrix} u(x + \Delta x, y + \Delta y, z + \Delta z) \\ v(x + \Delta x, y + \Delta y, z + \Delta z) \\ w(x + \Delta x, y + \Delta y, z + \Delta z) \end{pmatrix} &= \begin{pmatrix} u \\ v \\ w \end{pmatrix} + \begin{pmatrix} \partial u/\partial x & \partial u/\partial y & \partial u/\partial z \\ \partial v/\partial x & \partial v/\partial y & \partial v/\partial z \\ \partial w/\partial x & \partial w/\partial y & \partial w/\partial z \end{pmatrix} \begin{pmatrix} \Delta x \\ \Delta y \\ \Delta z \end{pmatrix} \\ &= \begin{pmatrix} u \\ v \\ w \end{pmatrix} + \begin{pmatrix} \Delta u \\ \Delta v \\ \Delta w \end{pmatrix}. \end{aligned} \quad (2.16)$$

Deformations are supposed to be small so that the principle of superposition holds.

From Eq. (2.16) it follows that the elongation of the face at  $z = 0$  in the  $x$ -direction is  $(\partial u/\partial x)dx$ , and accordingly that in the  $y$ -direction is  $(\partial v/\partial y)dy$ . The diagonal strain components are now defined as the relative elongations in the respective directions:

$$\varepsilon_{xx} = \varepsilon_{11} = \frac{\partial u}{\partial x}; \quad \varepsilon_{yy} = \varepsilon_{22} = \frac{\partial v}{\partial y}; \quad \varepsilon_{zz} = \varepsilon_{33} = \frac{\partial w}{\partial z}. \quad (2.17)$$

The shear strain characterizes the deformation of the quadratic faces into parallelograms. It is defined as the average of the two angles  $\beta \cong \partial u/\partial y$  and  $\alpha \cong \partial v/\partial x$  of the resulting parallelogram (see Fig. 2.4), i.e. as the average of the angular distortions of the  $z$ - $x$ -plane and the  $z$ - $y$ -plane:

$$\varepsilon_{xy} = \varepsilon_{12} = \frac{1}{2}(\alpha + \beta) = \frac{1}{2} \left( \frac{\partial u}{\partial y} + \frac{\partial v}{\partial x} \right). \quad (2.18)$$

Accordingly, for the other faces

$$\varepsilon_{xz} = \varepsilon_{13} = \frac{1}{2} \left( \frac{\partial u}{\partial z} + \frac{\partial w}{\partial x} \right), \quad (2.19)$$

$$\varepsilon_{yz} = \varepsilon_{23} = \frac{1}{2} \left( \frac{\partial v}{\partial z} + \frac{\partial w}{\partial y} \right). \quad (2.20)$$

Again, the symmetry relation

$$\varepsilon_{ij} = \varepsilon_{ji} \quad \text{for } i, j = 1, 2, 3 \quad (2.21)$$

holds because for non-rotating solid bodies (i.e. for bodies not exposed to additional centrifugal, centripetal or Coriolis forces)

$$\frac{\partial u}{\partial y} - \frac{\partial v}{\partial x} = \frac{\partial u}{\partial z} - \frac{\partial w}{\partial x} = \frac{\partial w}{\partial y} - \frac{\partial v}{\partial z} = 0. \quad (2.22)$$

In other words, without rotation,  $\varepsilon_{xy}$  and  $\varepsilon_{yx}$  are the average deformation angles for the same face and thus identical. Consequently, in Eq. (2.16) the mixed partial derivatives can be substituted by the average shear stresses, e.g.

$$\frac{\partial u}{\partial y} = \frac{1}{2} \left( \frac{\partial u}{\partial y} + \frac{\partial v}{\partial x} \right) = \varepsilon_{xy}.$$

Thus, the deformation equation (2.16) can be rewritten

$$\begin{pmatrix} \Delta u \\ \Delta v \\ \Delta w \end{pmatrix} = \begin{pmatrix} \varepsilon_{xx} & \varepsilon_{xy} & \varepsilon_{xz} \\ \varepsilon_{xy} & \varepsilon_{yy} & \varepsilon_{yz} \\ \varepsilon_{xz} & \varepsilon_{yz} & \varepsilon_{zz} \end{pmatrix} \begin{pmatrix} \Delta x \\ \Delta y \\ \Delta z \end{pmatrix} = \begin{pmatrix} \varepsilon_1 & \varepsilon_6 & \varepsilon_5 \\ \varepsilon_6 & \varepsilon_2 & \varepsilon_4 \\ \varepsilon_5 & \varepsilon_4 & \varepsilon_3 \end{pmatrix} \begin{pmatrix} \Delta x \\ \Delta y \\ \Delta z \end{pmatrix}. \quad (2.23)$$

The  $3 \times 3$  strain matrix  $\varepsilon = \{\varepsilon_{ij}\}$  is the representation of the strain tensor and – owing to the symmetry relation – can be reduced to the six-dimensional strain vector using again Voigt’s index correspondence (Table 2.1)

$$\bar{\varepsilon}^T = (\varepsilon_1, \varepsilon_2, \varepsilon_3, \varepsilon_4, \varepsilon_5, \varepsilon_6). \quad (2.24)$$

In engineering disciplines like structural mechanics the shear strain components are defined as twice the values used in physics and correspond to the values used in the torsion test of the section “Shear stresses”:

$$\gamma_{xy} = 2\varepsilon_{xy} = 2\varepsilon_6; \quad \gamma_{xz} = 2\varepsilon_{xz} = 2\varepsilon_5; \quad \gamma_{yz} = 2\varepsilon_{yz} = 2\varepsilon_4. \quad (2.25)$$

### The stress–strain relation for anisotropic materials

Assuming small deformations, the general relation between the strain and stress vectors (2.15) and (2.24) can be described by the linear equation

$$\bar{\sigma} = \mathbf{E} \cdot \bar{\varepsilon} + \bar{\alpha} \Delta T, \quad (2.26)$$

where  $\mathbf{E} = \{E_{ij}\}$  is the elasticity matrix with  $6 \times 6$  coefficients. The first contribution to the stress derives from the strain, but in the case of temperature differences  $\Delta T$  a temperature-induced stress term  $\bar{\alpha} \Delta T$  must be added. The vector  $\bar{\alpha}$  represents the thermal expansion coefficients

$$\bar{\alpha}^T = (\alpha_{xx}, \alpha_{yy}, \alpha_{zz}, \alpha_{yz}, \alpha_{xz}, \alpha_{xy}). \quad (2.27)$$

The incremental change of the elastic energy  $\delta U$  of a unit cube is given by the sum of the deformation work

$$2 \delta U = F_{xx} \delta \varepsilon_{xx} + F_{yy} \delta \varepsilon_{yy} + F_{zz} \delta \varepsilon_{zz} + F_{yz} \delta \varepsilon_{yz} + F_{xz} \delta \varepsilon_{xz} + F_{xy} \delta \varepsilon_{xy}. \quad (2.28)$$

The forces are given by the stress components  $F_{ij} = \sigma_{ij} dA$ . Owing to the identity of the mixed partial derivatives

$$2 \partial^2 U / \partial \varepsilon_{ij} \partial \varepsilon_{kl} = -\partial F_{ij} / \partial \varepsilon_{kl} = -\partial F_{kl} / \partial \varepsilon_{ij} \quad (2.29)$$

the matrix of elastic moduli is symmetric. Moreover, it has to be noted that the initial relation between the two  $3 \times 3$  strain and stress tensors of second order should be represented by a tensor of fourth order with  $9 \times 9 = 81$  coefficients. The symmetry relation of stress and strain has reduced this complexity to a tensor with 36 non-zero coefficients or to the equivalent compliance matrix with  $6 \times 6$  coefficients. The last symmetry consideration has decreased this number to 21. In the light of desired analytical expressions such a large number of entities is still difficult to handle. Fortunately, for most of the relevant materials used in MEMS technologies, additional symmetry relations hold, allowing us to reduce the number of non-zero coefficients further.

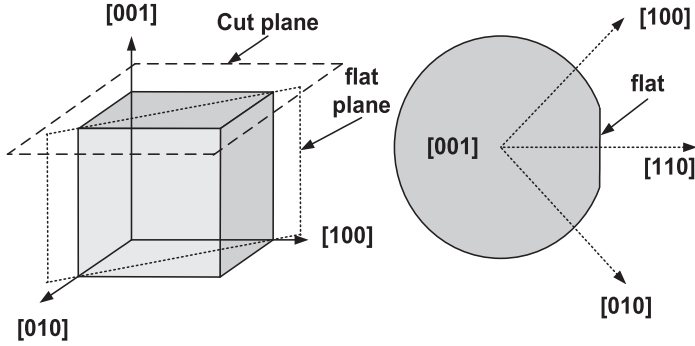


Figure 2.5 Silicon orientation on wafer.

### *The elasticity matrix of silicon*

As is well known, silicon has a diamond structure based on a cubic crystal lattice. The wafers used in microelectronics are usually cut along the (100) plane for CMOS and bulk micromachined devices.<sup>2</sup> As shown in Fig. 2.5 the surface of the wafer is in the (001) plane, and the orientation flat is directed in the [110] direction. This means that a device on the wafer that is orientated perpendicularly to the flat has an angle of  $45^\circ$  with the cube orientation axis [100].

If the different rotational and mirror symmetries of a cubic lattice are considered, the number of independent coefficients of the elasticity matrix reduces from 21 to 3. The elasticity matrix for a material under stress, orientated along the [100] axis, is

$$\mathbf{E} = \begin{pmatrix} E_{11} & E_{12} & E_{12} & 0 & 0 & 0 \\ E_{12} & E_{11} & E_{12} & 0 & 0 & 0 \\ E_{12} & E_{12} & E_{11} & 0 & 0 & 0 \\ 0 & 0 & 0 & E_{44} & 0 & 0 \\ 0 & 0 & 0 & 0 & E_{44} & 0 \\ 0 & 0 & 0 & 0 & 0 & E_{44} \end{pmatrix} \quad (2.30)$$

with only 12 non-zero moduli of elasticity. This structure reflects a general property of a parameter matrix of anisotropic materials with cubic symmetry and holds, for instance, also for the parameters describing the piezoresistivity effect.

For stress orientations differing from the [100] axis, the coefficients of the rotated matrix have to be calculated. This will be done in Section 2.1.2.

The inverse relation between stress and strain can be described by the compliance matrix, which is the inverse of the matrix of elastic moduli:

$$\bar{\epsilon} = \mathbf{S} \cdot (\bar{\sigma} - \bar{\alpha} \Delta T). \quad (2.31)$$

<sup>2</sup> (100) Planes are perpendicular to [100] directions. The set of six equivalent directions is denoted by  $\langle 100 \rangle$ , and the set of equivalent planes by  $\{100\}$ .

$\mathbf{S} = \{s_{ij}\}$  has the same structure as the  $\mathbf{E}$  matrix,

$$\mathbf{S} = \begin{pmatrix} s_{11} & s_{12} & s_{12} & 0 & 0 & 0 \\ s_{12} & s_{11} & s_{12} & 0 & 0 & 0 \\ s_{12} & s_{12} & s_{11} & 0 & 0 & 0 \\ 0 & 0 & 0 & s_{44} & 0 & 0 \\ 0 & 0 & 0 & 0 & s_{44} & 0 \\ 0 & 0 & 0 & 0 & 0 & s_{44} \end{pmatrix} = \mathbf{E}^{-1}, \quad (2.32)$$

with the following coefficients:

$$s_{11} = \frac{1}{E}; \quad s_{12} = -\frac{\nu}{E}; \quad s_{44} = \frac{1}{2G}. \quad (2.33)$$

$E$  and  $\nu$  are the Hookean Young modulus and Poisson ratio.  $G$  is the shear modulus or modulus of rigidity, defined by the ratio

$$G = \frac{\sigma_{ij}}{2\varepsilon_{ij}}, \quad i \neq j. \quad (2.34)$$

For silicon, the following data, referred to the [100] crystal orientation, are usually quoted [Gad-el-Hak 2002, Brantley 1973]:

$$\begin{aligned} E = \frac{1}{s_{11}} = 131 \text{ GPa}; & \quad \nu = -\frac{s_{12}}{s_{11}} = 0.28; & \quad G = \frac{1}{2s_{44}} = 80 \text{ GPa}; \\ E_{11} = 166 \text{ GPa}; & \quad E_{12} = 64 \text{ GPa}; & \quad E_{44} = 80 \text{ GPa}. \end{aligned} \quad (2.35)$$

Despite its significantly lower yield and fracture strength, a mechanically isotropic polysilicon layer has elastic properties similar those of to bulk silicon. The Young modulus is usually specified as  $E_{\text{poly}} = 160 \text{ MPa}$ , and the Poisson ratio  $\nu_{\text{poly}} = 0.23$ ; however, the spread within materials with different grain structures may be quite significant, and also the spread within different dies need not be negligible.

To get a feeling for the orders of magnitude, a very simple example is considered. A silicon cube of dimensions  $1 \text{ cm} \times 1 \text{ cm} \times 1 \text{ cm}$  is loaded with  $1000 \text{ kg}$  on the top face. The cube is then compressed by  $0.07\%$  or  $7 \mu\text{m}$ , and the lateral extension is  $0.02\%$  or  $2\mu\text{m}$ .

### *Elasticity of isotropic materials*

For isotropic materials the structure of Eqs. (2.26) and (2.31) does not change. However,  $G$  is no longer an independent parameter, but given by the relation [Macke 1962, Chou and Pagano 1967]

$$G = \frac{E}{2(1 + \nu)}. \quad (2.36)$$

This equation follows from the anisotropy definition

$$\alpha_{\text{anisotropy}} = \frac{2E_{44}}{E_{11} - E_{12}}, \quad (2.37)$$

which for isotropic materials ( $\alpha_{\text{anisotropy}} = 1$ ) fixes the interrelation among  $E_{11}$ ,  $E_{12}$ , and  $E_{44}$ . It can also be derived from the identity of the principal stress and strain axes in isotropic bodies.<sup>3</sup>

### *Elastic strain energy*

If stress and strain within a material are known, it is often convenient to represent the status by the elastic strain energy  $U_{\text{elastic}}$  within a given volume  $V$ . Equilibrium states can be found by minimizing the energy, forces can be derived as gradients of the energy, and so on. The elastic energy  $U_{\text{elastic}}$  is the accumulated work for the generation of all displacements, i.e. the sum of all displacements multiplied by the forces needed for this displacement:

$$\begin{aligned} U_{\text{elastic}} &= \frac{1}{2} \sum_{i,j} \int \int \int_V \varepsilon_{ij} \sigma_{ij} \, dx \, dy \, dz \\ &= \frac{1}{2} \int_V dV (\sigma_x \varepsilon_x + \sigma_y \varepsilon_y + \sigma_z \varepsilon_z + 2\sigma_{xy} \varepsilon_{xy} + 2\sigma_{xz} \varepsilon_{xz} + 2\sigma_{yz} \varepsilon_{yz}). \end{aligned} \quad (2.38)$$

For isotropic materials the application of Hooke's law yields

$$\begin{aligned} U_{\text{elastic}} &= \frac{1}{2} \int_V dV \left\{ \frac{1}{E} [\sigma_x^2 + \sigma_y^2 + \sigma_z^2 - 2\nu(\sigma_x \sigma_y + \sigma_x \sigma_z + \sigma_y \sigma_z)] \right. \\ &\quad \left. + \frac{1}{G} (\sigma_{xy}^2 + \sigma_{xz}^2 + \sigma_{yz}^2) \right\}. \end{aligned} \quad (2.39)$$

### **The piezoresistance of silicon**

Piezoresistors are excellent stress transducers and have found broad application within inertial MEMS. They change their resistance depending on the applied stress.

The material laws of Maxwell's equation state that the electrical field  $\bar{E}$  and current density  $\bar{J}$  in an isotropic medium relate to each other as

$$\bar{E} = \rho \bar{J} \quad \text{and} \quad \bar{J} = \sigma \bar{E} \quad \text{where} \quad \sigma = \frac{1}{\rho}. \quad (2.40)$$

Here  $\rho$  is the resistivity and  $\sigma$  the conductivity of the material. In silicon or other crystals resistivity and conductivity are anisotropic;  $\rho$  and  $\sigma$  become tensors of second order, e.g.

$$\bar{E} = \rho \bar{J} \quad \Rightarrow \quad \begin{pmatrix} E_x \\ E_y \\ E_z \end{pmatrix} = \begin{pmatrix} \rho_{xx} & \rho_{xy} & \rho_{xz} \\ \rho_{xy} & \rho_{yy} & \rho_{yz} \\ \rho_{xz} & \rho_{yz} & \rho_{zz} \end{pmatrix} \begin{pmatrix} J_x \\ J_y \\ J_z \end{pmatrix}. \quad (2.41)$$

Here the symmetry relations  $\rho_{ij} = \rho_{ji}$ ,  $i \neq j$ , were used [Smith 1958, Nye 1985]. Using again Voigt's notation  $\rho_1 = \rho_{xx}$ ,  $\rho_2 = \rho_{yy}$ ,  $\rho_3 = \rho_{zz}$ ,  $\rho_4 = \rho_{yz}$ ,  $\rho_5 = \rho_{xz}$ ,

<sup>3</sup> The principal stress (strain) axes are defined by coordinate systems at the point  $P(x, y, z)$ , for which the shear-stress (shear-strain) components vanish.

**Table 2.2.** Piezoresistivity coefficients for high-resistivity silicon in units of  $(100 \text{ GPa})^{-1}$ 

	$\rho_0$ ( $\Omega \text{ cm}$ )	$\pi_{11}$	$\pi_{12}$	$\pi_{44}$
p-Silicon	7.8	6.6	-1.12	138.1
n-Silicon	11.7	-102.2	53.4	-13.6

and  $\rho_6 = \rho_{xy}$ , the resistivity can be expressed as the sum of the resistivity component in the absence of stress plus the changes induced by the stress<sup>4</sup>

$$\begin{pmatrix} \rho_1 \\ \rho_2 \\ \rho_3 \\ \rho_4 \\ \rho_5 \\ \rho_6 \end{pmatrix} = \begin{pmatrix} \rho_0 \\ \rho_0 \\ \rho_0 \\ 0 \\ 0 \\ 0 \end{pmatrix} + \rho_0 \begin{pmatrix} \pi_{11} & \pi_{12} & \pi_{12} & 0 & 0 & 0 \\ \pi_{12} & \pi_{11} & \pi_{12} & 0 & 0 & 0 \\ \pi_{12} & \pi_{12} & \pi_{22} & 0 & 0 & 0 \\ 0 & 0 & 0 & \pi_{44} & 0 & 0 \\ 0 & 0 & 0 & 0 & \pi_{44} & 0 \\ 0 & 0 & 0 & 0 & 0 & \pi_{44} \end{pmatrix} \begin{pmatrix} \sigma_1 \\ \sigma_2 \\ \sigma_3 \\ \sigma_4 \\ \sigma_5 \\ \sigma_6 \end{pmatrix}. \quad (2.42)$$

As before, the symmetries of a cubic crystal with its axis aligned along the  $\langle 100 \rangle$  axis were taken into consideration. The  $\pi_{ij}$  are the coefficients of the piezoresistivity tensor and are usually cited from Smith's early work [Smith 1954], as shown in Table 2.2. For p-Si the approximation  $\pi_{11} = \pi_{12} = 0$  is often used, and for n-Si  $\pi_{11} = -2\pi_{12}$ ;  $\pi_{44} = 0$ .

At high temperatures doped piezoresistor structures on bulk silicon are corrupted by leakage currents to the substrate, which limits their applicability. Isolated polysilicon layers eliminate this drawback and are a useful alternative to crystalline silicon. The polysilicon layer always has a random grain distribution in the  $x$ - $y$ -plane. There may be preferred  $z$ -orientations of the grains. In any case, the piezoresistivity coefficients for a planar piezoresistor with arbitrary orientation have to be calculated by taking the average of the piezo-coefficients over all grains and grain orientations. This task can be simplified considerably by considering only thin resistors with negligible height, as is the case in piezoresistive MEMS transducers (see Section 2.2.1).

### 2.1.2 Rotation of coordinate systems

There are two occasions when the mathematical tools for describing the rotation of coordinate systems are needed.

- The orientation-dependency of stress, strain, and anisotropic material properties. Here, the two coordinate systems have fixed, time-independent orientations.

<sup>4</sup> The components of the stress tensor  $\sigma_i$  should not be confused with the notation for the conductivity of the isotropic medium  $\sigma$ .

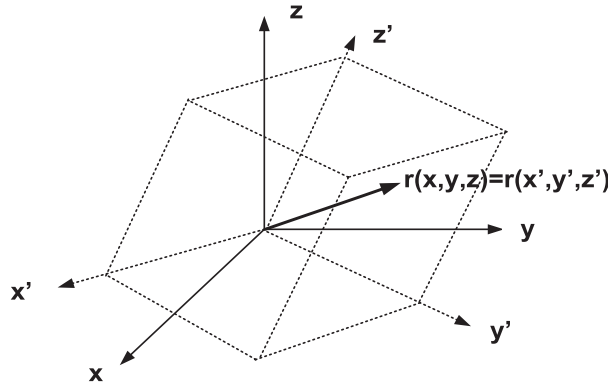


**Figure 2.6** A vector in two different coordinate systems.

- The rotation as source of virtual inertial forces, e.g. for the description of the dynamics of gyroscopes. Here, one coordinate system rotates with respect to another with a certain, non-zero, speed.

In this subsection the static transformation rules for vectors and tensors of second order in rotated coordinate systems are considered. In view of dynamic effects this subsection is formulated in a way that allows a natural extension towards rotating coordinate systems as considered in Chapter 8.

### Coordinate frames

In Fig. 2.6 the vector  $\bar{r}$  is represented in two different coordinate systems  $\bar{E}_x, \bar{E}_y, \bar{E}_z$  and  $\bar{e}_x, \bar{e}_y, \bar{e}_z$ , which have the same origin but are rotated with respect to each other. More precisely, the two coordinate frames before –  $\Sigma_E$  – and after –  $\Sigma_e$  – rotation are defined by their basis vectors

$$\Sigma_E: \underline{\bar{E}}^T = [\bar{E}_1, \bar{E}_2, \bar{E}_3] \quad \text{and} \quad \Sigma_e: \underline{\bar{e}}^T = [\bar{e}_1, \bar{e}_2, \bar{e}_3], \quad (2.43)$$

which are orthonormal, e.g.  $\bar{E}_i^T \bar{E}_j = \delta_{ij}$ , and satisfy the right-handedness condition: e.g.  $\bar{E}_1^T \bar{E}_2 \times \bar{E}_3 = +1$ .  $\bar{A} \cdot \bar{B} = \bar{A}^T \bar{B}$  is the scalar or dot product of two vectors  $\bar{A} = [A_1, A_2, A_3]^T$  and  $\bar{B} = [B_1, B_2, B_3]^T$ .  $\bar{A} \times \bar{B}$  is their vector product. The superscript T denotes a vector or matrix transposition, and  $\delta_{ij}$  is the Kronecker symbol. Underlined letters characterize a column arrangement of corresponding items, in Eq. (2.43), of the vectors  $\bar{e}_i$ . The product of a matrix  $\mathbf{D}$  with an underlined vector,  $\mathbf{D}\underline{u}$ , is interpreted as a usual matrix multiplication irrespective of whether the elements of  $\underline{u}$  are numbers or vectors.

The orthonormality of the base yields

$$\underline{\bar{E}} \cdot \underline{\bar{E}}^T = \underline{\bar{E}}^T \underline{\bar{E}} = \underline{\bar{e}} \cdot \underline{\bar{e}}^T = \underline{\bar{e}}^T \underline{\bar{e}} = I, \quad (2.44)$$

where  $I$  is the unit matrix.

Here,  $\bar{A}\bar{B}^T = \bar{A} \otimes \bar{B}$  is interpreted as the dyadic product of the vectors  $\bar{A}$  and  $\bar{B}$ . The dyadic product of  $\bar{A}^T = [A_1, A_2, A_3]$  and  $\bar{B}^T = [B_1, B_2, B_3]$  is defined by

$$\bar{A} \otimes \bar{B} = \begin{pmatrix} A_1 B_1 & A_1 B_2 & A_1 B_3 \\ A_2 B_1 & A_2 B_2 & A_2 B_3 \\ A_3 B_1 & A_3 B_2 & A_3 B_3 \end{pmatrix}. \quad (2.45)$$

The dot sign between the vectors in Eq. (2.44) means that the components of the dyadic product are connected by scalar multiplication.

The vector  $\bar{r}$  is seen as the same entity in both coordinate systems and remains unchanged. Thus

$$\bar{r} = \sum_i r_{E,i} \bar{E}_i = \sum_i r_{e,i} \bar{e}_i. \quad (2.46)$$

For convenience the column vectors  $\underline{r}_E$  and  $\underline{r}_e$  are introduced:

$$\underline{r}_E = [r_{E,1}, r_{E,2}, r_{E,3}]^T; \quad \underline{r}_e = [r_{e,1}, r_{e,2}, r_{e,3}]^T. \quad (2.47)$$

They represent the vectors of coordinates of  $\bar{r}$  in  $\Sigma_E$  and in  $\Sigma_e$ , respectively, and should not be confused with the actual vector  $\bar{r}$  itself, which can now be represented in a compact form:

$$\bar{r} = \underline{\bar{E}}^T \underline{r}_E = \underline{\bar{e}}^T \underline{r}_e, \quad \bar{r}_E = \underline{\bar{E}} \bar{r} \quad \text{and} \quad \bar{r}_e = \underline{\bar{e}} \bar{r}. \quad (2.48)$$

The tensor concept should be briefly evoked. A tensor  $\mathbb{K}$  of second order is an arrangement of vectors according to the following scheme:

$$\mathbb{K} = \underline{\bar{E}}^T \mathbf{K}^E \underline{\bar{E}} = \left\{ \sum_i \sum_j K_{ij}^E \bar{E}_i \bar{E}_j \right\} = \underline{\bar{e}}^T \mathbf{K}^e \underline{\bar{e}} = \left\{ \sum_i \sum_j K_{ij}^e \bar{e}_i \bar{e}_j \right\}. \quad (2.49)$$

It allows us to express vector relations independently of their representation in different coordinate systems. The corresponding coordinate matrices  $\mathbf{K}^E$  and  $\mathbf{K}^e$  in two different  $\underline{\bar{E}}$  and  $\underline{\bar{e}}$  are defined by the equality (2.49). On applying a tensor to a vector  $\bar{r}$ , say within the coordinate system  $\underline{\bar{E}}$ :  $\bar{r} = \underline{\bar{E}}^T \underline{r}_E$ , one gets

$$\mathbb{K} \cdot \bar{r} = \underline{\bar{E}}^T \mathbf{K}^E \underline{\bar{E}} \cdot \underline{\bar{E}}^T \underline{r}_E = \underline{\bar{E}}^T \mathbf{K}^E \underline{r}_E. \quad (2.50)$$

This means that the application of a tensor to a vector within a given coordinate system transforms the coordinate vector within this system by matrix multiplication with the coordinate matrix of the tensor represented within the same coordinate system.

### The rotation tensor

The tensor of rotation represented by its coefficient matrix in  $\Sigma_e$ , namely  $\mathbb{S} = \underline{\bar{e}}^T \mathbf{S} \underline{\bar{e}}$ , rotates the unit vectors of  $\Sigma_E$  into the unit vectors of  $\Sigma_e$ . Strictly speaking, the rotation matrix  $\mathbf{S}$  should be labeled by the superscript  $E$ , which will be omitted.

The rotation is determined by

$$\underline{\bar{e}} = \mathbf{S}\underline{\bar{E}} \quad \text{or} \quad \bar{e}_i = \sum_j \hat{S}_{ij} \bar{E}_j. \quad (2.51)$$

By means of right-hand multiplication of the first equation with  $\underline{\bar{E}}^T$  the rotation matrix  $\mathbf{S}$  can be explicitly written

$$\mathbf{S} = \underline{\bar{e}} \underline{\bar{E}}^T. \quad (2.52)$$

Equations (2.48) and (2.52) deliver immediately

$$r_E = \mathbf{S}^T r_e \quad \text{and correspondingly} \quad r_e = \mathbf{S} r_E. \quad (2.53)$$

The coefficients of the matrix  $\mathbf{S} = \{\hat{S}_{ij}\}$  follow from the second equation in (2.51) after transposition and right-hand multiplication with  $\bar{E}_k$ ,

$$\hat{S}_{i,j} = \bar{e}_i^T \bar{E}_j. \quad (2.54)$$

The scalar product  $\bar{e}_i^T \bar{E}_j$  is the direction cosine, i.e. the projection of  $\bar{e}_i$  onto  $\bar{E}_j$ .

The inverse rotation is, by definition,  $\mathbf{S}^{-1} = \underline{\bar{E}} \underline{\bar{e}}^T = (\underline{\bar{e}} \underline{\bar{E}}^T)^T = \mathbf{S}^T$ . Thus,

$$\mathbf{S}^{-1} = \mathbf{S}^T. \quad (2.55)$$

Additionally, it is easy to show that  $\det \mathbf{S} = +1$ . Analogous equations are valid for all tensors of rotation.

Since  $\mathbf{S}^T \mathbf{S} = \mathbf{I}$ , where  $\mathbf{I}$  is the unit matrix, it follows that

$$\sum_k \hat{S}_{k,i} \hat{S}_{k,j} = \delta_{ij} \quad \Rightarrow \quad \sum_k \hat{S}_{k,i}^2 = \sum_k \hat{S}_{i,k}^2 = 1. \quad (2.56)$$

This equation may be useful; it reduces the nine directional cosines to the three independent values.

### *Separation of partial rotations – Euler angles*

In order to derive the coefficients of the matrix  $\mathbf{S}$ , the projections according to (2.54) have to be calculated. The most convenient way to do this goes back to Euler. Euler partitioned the whole rotation into three partial rotations, each partial rotation taking place about a well-defined axis by a certain angle. The fact that any rotation can be partitioned into three subsequent rotations shows that the matrix  $\mathbf{S}$  has only three independent parameters. There are different ways to define the sequence of partial rotations to get a total rotation. Euler introduced the so-called standard Euler angles  $\phi$ ,  $\theta$ , and  $\psi$  for the following (standard) sequence of rotations.

- First, counterclockwise rotation about the  $z$ -axis ( $\bar{E}_3$ -axis) of the initial coordinate system by the angle  $\phi$ , transforming the coordinates of a vector endpoint  $(r_1, r_2, r_3)$  into the new coordinates  $(r_1^{\{1\}}, r_2^{\{1\}}, r_3^{\{1\}} = r_3)$ .
- Second, counterclockwise rotation about the new  $\bar{E}_2^{\{1\}}$ -axis by the angle  $\theta$ . This rotation transforms the coordinates  $(r_1^{\{1\}}, r_2^{\{1\}}, r_3^{\{1\}})$  into  $(r_1^{\{2\}}, r_2^{\{2\}} = r_2^{\{1\}}, r_3^{\{2\}})$ .

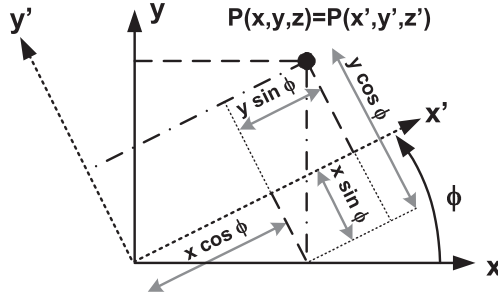


**Figure 2.7**  $z$ -Rotation of the  $x$ - $y$ -coordinate system.  $x' = x \cos \phi + y \sin \phi$ ,  $y' = -x \sin \phi + y \cos \phi$ ,  $z' = z$ , and  $\phi = \theta_3$ .

- Third, counterclockwise rotation about the new  $\bar{E}_3^{\{2\}}$ -axis by the angle  $\psi$ . This rotation transforms the coordinates  $(r_1^{\{2\}}, r_2^{\{2\}}, r_3^{\{2\}})$  into the final coordinates  $(r_1^{\{3\}} = r_1', r_2^{\{3\}} = r_2', r_3^{\{3\}} = r_3^{\{2\}} = r_3')$ .

The described sequence converts the coordinate frames step by step according to  $\Sigma_E \rightarrow \Sigma_E^{\{1\}} \rightarrow \Sigma_E^{\{2\}} \rightarrow \Sigma_E^{\{3\}} = \Sigma_e$ . The triad of vectors  $(\bar{E}_3, \bar{E}_2^{\{1\}}, \bar{E}_3^{\{2\}})$  is called the Euler basis.<sup>5</sup>

### Bryan angles

Throughout this book the Bryan or Cardan angles (e.g. [Wittenburg \[2008\]](#)) are used. They are represented by slightly modified, non-standard Euler angles  $\psi_1, \psi_2, \psi_3$ . Their corresponding Euler basis is

$$(\bar{E}_1, \bar{E}_2^{\{1\}}, \bar{E}_3^{\{2\}}), \quad (2.57)$$

i.e. the first counterclockwise rotation is about the  $x$ -axis by  $\psi_1 = \psi_x$ , the second about the  $y$ -axis of the rotated frame by  $\psi_2 = \psi_y$ , and the third about the  $z$ -axis of the secondly rotated coordinate system by  $\psi_3 = \psi_z$ . In a rotation sequence – starting with rotation about the  $x$ -axis – only the third rotation differs from a standard Euler sequence.

All coordinate transformations follow the same rules. For example, the third rotation about the  $z$ -axis by the angle  $\psi_3$ , shown in Fig. 2.7, transforms the coordinates of a given vector endpoint according to

$$\begin{pmatrix} x^{\{1\}} \\ y^{\{1\}} \\ z^{\{1\}} \end{pmatrix} = \begin{pmatrix} c_{\theta_3} & s_{\theta_3} & 0 \\ -s_{\theta_3} & c_{\theta_3} & 0 \\ 0 & 0 & 1 \end{pmatrix} \begin{pmatrix} x \\ y \\ z \end{pmatrix} = \mathbf{S}_3(\psi_3). \quad (2.58)$$

Throughout this text the abbreviations  $s_\alpha$  for  $\sin \alpha$  and  $c_\alpha$  for  $\cos \alpha$  shall be used. Correspondingly, in cases of unambiguity  $\sin \psi_i = s_i$  and  $\cos \psi_i = c_i$ . The

<sup>5</sup> There are different standard Euler bases. So, the sequence of rotations may start from any of the axes. For the second rotation there are always two possibilities. The only requirement is the identity of the first and third rotational matrices.

following transformations can be derived by a simple cyclic permutation of the axes of the coordinate system, i.e. for the second rotation by the permutation  $z \Rightarrow y; y \Rightarrow x; x \Rightarrow z$ . The following sequence of transformations results:

$$\begin{aligned}\underline{r}^{\{1\}} &= \mathbf{S}_1(\psi_1)\underline{r}, \\ \underline{r}^{\{2\}} &= \mathbf{S}_2(\psi_2)\underline{r}^{\{1\}}, \\ \underline{r}^{\{3\}} &= \mathbf{S}_3(\psi_3)\underline{r}^{\{2\}} = \underline{r}',\end{aligned}\tag{2.59}$$

where the partial transformations are defined by

$$\mathbf{S}_3(\psi_3) = \begin{pmatrix} c_3 & s_3 & 0 \\ -s_3 & c_3 & 0 \\ 0 & 0 & 1 \end{pmatrix}; \quad \mathbf{S}_2(\psi_2) = \begin{pmatrix} c_2 & 0 & -s_2 \\ 0 & 1 & 0 \\ s_2 & 0 & c_2 \end{pmatrix}; \quad \mathbf{S}_1(\psi_1) = \begin{pmatrix} 1 & 0 & 0 \\ 0 & c_1 & s_1 \\ 0 & -s_1 & c_1 \end{pmatrix}.\tag{2.60}$$

The overall coordinate transformation can now be written as

$$\underline{r}_e = \underline{r}^{\{3\}} = \mathbf{S}_3(\psi_3)\mathbf{S}_2(\psi_2)\mathbf{S}_1(\psi_1)\underline{r}_E = \mathbf{S}\underline{r}_E,\tag{2.61}$$

with

$$\begin{aligned}\mathbf{S}(\psi_1, \psi_2, \psi_3) &= \{\hat{S}_{ij}\} = \begin{pmatrix} c_3 c_2 & c_3 s_2 s_1 + s_3 c_1 & -c_3 s_2 c_1 + s_3 s_1 \\ -s_3 c_2 & -s_3 s_2 s_1 + c_3 c_1 & s_3 s_2 c_1 + c_3 s_1 \\ s_2 & -c_2 s_1 & c_2 c_1 \end{pmatrix} \\ &= \begin{pmatrix} l_1 & m_1 & n_1 \\ l_2 & m_2 & n_2 \\ l_3 & m_3 & n_3 \end{pmatrix}.\end{aligned}\tag{2.62}$$

In contrast to Euler angles, the Bryan angles give one the possibility to linearize the rotation matrix  $R$  about the zero angles, while the Euler transformation consists of members of order  $\psi_i \psi_j$  and higher with missing linear terms.

Instead of doubly subscripted coefficients  $\hat{S}_{i,j}$ , it is convenient to introduce the factors  $l_i, m_i$ , and  $n_i$ , for the sake of visual clarity (e.g. [Gad-el-Hak \[2002\]](#)). The reader should be reminded that, according to Eq. (2.56), the sum of the squares along a column or a row is equal to one.

### Transformation of tensors of second order

Up to now the transformation of vectors between rotated frames has been considered. However, the consideration of elasticity, piezoelectricity, moments of inertia, and so on requires the description of material properties governed by second-order tensors (or matrices) within rotated coordinate systems. Piezo-resistivity may serve as a representative example for the transformation of material properties from one coordinate system into another.

According to (2.40),

$$\bar{E} = \rho \bar{J},\tag{2.63}$$

the relation between the electrical field  $\bar{E}$  and current density  $\bar{J}$  within an anisotropic material, is valid in a given coordinate frame  $\Sigma$ . In the case of orientation-dependent properties such as piezoresistance this coordinate system is inseparably linked to the material orientation, here to the (100) plane and [100] axis of the cubic silicon crystal. If the material which possesses orientation-dependent properties is rotated with respect to the applied field or current (or vice versa), the impact of the material properties changes. In order to describe these changes,  $\bar{E}$  and  $\bar{J}$  have to be expressed in the rotated coordinate system.

With the fields  $\bar{E}' = \mathbf{S}\bar{E}$  and  $\bar{J}' = \mathbf{S}\bar{J}$  in the rotated frame  $\Sigma'$ , Eq. (2.63) can be rewritten using property (2.55) as

$$\bar{E}' = \mathbf{S}\boldsymbol{\rho}\mathbf{S}^T \bar{J}' = \boldsymbol{\rho}' \bar{J}'. \quad (2.64)$$

Thus, the coordinate matrix of the resistivity tensor  $\boldsymbol{\rho}'$  in the rotated coordinate system is

$$\boldsymbol{\rho}' = \mathbf{S}\boldsymbol{\rho}\mathbf{S}^T. \quad (2.65)$$

Since the new matrix  $\{\rho'_{ij}\}$  is also symmetric and, thus, has only six known independent components, Voigt's notation can be applied, transforming  $\boldsymbol{\rho}'$  into the vector representation  $\bar{\rho}'^T = [\rho'_1 = \rho'_{xx}, \rho'_2 = \rho'_{yy}, \rho'_3 = \rho'_{zz}, \rho'_4 = \rho'_{yz}, \rho'_5 = \rho'_{xz}, \rho'_6 = \rho'_{xy}]$ . On performing this slightly cumbersome transformation for the matrix equation (2.65), one obtains

$$\bar{\rho}' = \boldsymbol{\Gamma}\bar{\rho}, \quad (2.66)$$

where  $\boldsymbol{\Gamma}$  is defined by

$$\boldsymbol{\Gamma} = \begin{pmatrix} l_1^2 & m_1^2 & n_1^2 & 2m_1n_1 & 2l_1n_1 & 2l_1m_1 \\ l_2^2 & m_2^2 & n_2^2 & 2m_2n_2 & 2l_2n_2 & 2l_2m_2 \\ l_3^2 & m_3^2 & n_3^2 & 2m_3n_3 & 2l_3n_3 & 2l_3m_3 \\ l_2l_3 & m_2m_3 & n_2n_3 & m_2n_3 + m_3n_2 & n_2l_3 + n_3l_2 & m_2l_3 + m_3l_2 \\ l_1l_3 & m_1m_3 & n_1n_3 & m_3n_1 + m_1n_3 & n_3l_1 + n_1l_3 & m_3l_1 + m_1l_3 \\ l_1l_2 & m_1m_2 & n_1n_2 & m_1n_2 + m_2n_1 & n_1l_2 + n_2l_1 & m_1l_2 + m_2l_1 \end{pmatrix}. \quad (2.67)$$

The matrix of piezo-coefficients in Eq. (2.42),

$$\boldsymbol{\Pi} = \begin{pmatrix} \pi_{11} & \pi_{12} & \pi_{12} & 0 & 0 & 0 \\ \pi_{12} & \pi_{11} & \pi_{12} & 0 & 0 & 0 \\ \pi_{12} & \pi_{12} & \pi_{22} & 0 & 0 & 0 \\ 0 & 0 & 0 & \pi_{44} & 0 & 0 \\ 0 & 0 & 0 & 0 & \pi_{44} & 0 \\ 0 & 0 & 0 & 0 & 0 & \pi_{44} \end{pmatrix}, \quad (2.68)$$

represents a tensor of fourth order relating the two tensors of second order, namely the stress tensor  $\sigma$  and the resistivity tensor  $\rho$ ; more precisely it represents the tensor of resistivity changes  $\Delta\rho$  under stress:

$$\Delta\rho = \frac{\rho - \rho_0\mathbf{I}}{\rho_0} = \boldsymbol{\Pi}\sigma. \quad (2.69)$$

The vector representation of the tensors of second order  $\sigma$  and  $\rho$  by  $\bar{\sigma}^T = (\sigma_1, \sigma_2, \sigma_3, \sigma_4, \sigma_5, \sigma_6)$  and  $\bar{\rho}$  allows us to describe the transformation of the tensor coefficients for a rotation of the coordinate system by a simple matrix relation:

$$\bar{\rho}' = \mathbf{\Gamma} \bar{\rho}; \quad \bar{\Delta}' \rho = \mathbf{\Gamma} \bar{\Delta} \rho; \quad \bar{\sigma}' = \mathbf{\Gamma} \bar{\sigma}. \quad (2.70)$$

On substituting these expressions into Eq. (2.69) it follows that

$$\Delta' \rho = \mathbf{\Gamma} \mathbf{\Pi} \mathbf{\Gamma}^{-1} \sigma'. \quad (2.71)$$

Consequently, the piezoresistive tensor in the rotated coordinate system is given by the matrix

$$\mathbf{\Pi}' = \mathbf{\Gamma} \mathbf{\Pi} \mathbf{\Gamma}^{-1}. \quad (2.72)$$

Unfortunately, during the transfer of second-order tensors to vectors the nice unitarity property of the rotation tensor  $\mathbf{S}^{-1} = \mathbf{S}^T$  has not been handed over to the corresponding matrix  $\mathbf{\Gamma}$ .  $\mathbf{\Gamma}^{-1}$  must be calculated straightforwardly:

$$\mathbf{\Gamma}^{-1} = \begin{pmatrix} l_1^2 & l_2^2 & l_3^2 & 2l_2l_3 & 2l_1l_3 & 2l_1l_2 \\ m_1^2 & m_2^2 & m_3^2 & 2m_2m_3 & 2m_1m_3 & 2m_1m_2 \\ n_1^2 & n_2^2 & n_3^2 & 2n_2n_3 & 2n_1n_3 & 2n_1n_2 \\ m_1n_1 & m_2n_2 & m_3n_3 & m_2n_3 + m_3n_2 & m_3n_1 + m_1n_3 & m_1n_2 + m_2n_1 \\ l_1n_1 & l_2n_2 & l_3n_3 & n_2l_3 + n_3l_2 & l_1n_3 + l_3n_1 & n_1l_2 + n_2l_1 \\ l_1m_1 & l_2m_2 & l_3m_3 & m_2l_3 + m_3l_2 & l_1m_3 + l_3m_1 & m_1l_2 + m_2l_1 \end{pmatrix}. \quad (2.73)$$

In summary, the rotated matrix of piezo-coefficients  $\mathbf{\Pi}'$  no longer has only 12 non-zero components, but, rather, all 36 are now non-vanishing. The calculation of  $\mathbf{\Pi}'$  is simplified by the block structure of  $\mathbf{\Gamma}$  as well as of  $\mathbf{\Pi}$ . For the most important cases, where the coordinate system is rotated only about the axis perpendicular to the (100) plane of silicon by the angle  $\psi_3$ , the angles are  $\psi_2 = 0$  and  $\psi_1 = 0$ , so that

$$\{\pi'_{ij}\} = \begin{pmatrix} \pi_{11} - \frac{1}{2}\pi_0 \sin^2(2\psi_3) & \pi_{11} + \frac{1}{2}\pi_0 \sin^2(2\psi_3) & \pi_{12} & 0 & 0 & -\frac{1}{2}\pi_0 \sin(4\psi_3) \\ \pi_{11} + \frac{1}{2}\pi_0 \sin^2(2\psi_3) & \pi_{11} - \frac{1}{2}\pi_0 \sin^2(2\psi_3) & \pi_{12} & 0 & 0 & \frac{1}{2}\pi_0 \sin(4\psi_3) \\ \pi_{12} & \pi_{12} & \pi_{11} & 0 & 0 & 0 \\ 0 & 0 & 0 & \pi_{44} & 0 & 0 \\ 0 & 0 & 0 & 0 & \pi_{44} & 0 \\ -\frac{1}{4}\pi_0 \sin(4\psi_3) & \frac{1}{2}\pi_0 \sin(4\psi_3) & 0 & 0 & 0 & \pi_{44} + \pi_0 \sin^2(2\psi_3) \end{pmatrix}, \quad (2.74)$$

where

$$\pi_0 = \pi_{11} - \pi_{12} - \pi_{44}. \quad (2.75)$$